HHS Public Access

Author manuscript

Prog Retin Eye Res. Author manuscript; available in PMC 2020 October 15.

Published in final edited form as:

Prog Retin Eye Res. 2020 January ; 74: 100774. doi:10.1016/j.preteyeres.2019.100774.

Lessons learned from quantitative fundus autofluorescence

Janet R. Sparrow[a,b,*,1], **Tobias Duncker**[a,1], **Kaspar Schuerch**[a,1], **Maarjaliis Paavo**[a,1], **Jose Ronaldo Lima de Carvalho Jr.**[a,c,d,1]

[a]Department of Ophthalmology, Columbia University, New York, NY, USA

[b]Department of Pathology and Cell Biology, Columbia University, New York, NY, USA

[c]Departament of Ophthalmology, Hospital das Clinicas de Pernambuco (HCPE) - Empresa Brasileira de Servicos Hospitalares (EBSERH), Federal University of Pernambuco (UFPE), Recife, Pernambuco, Brazil

[d]Department of Ophthalmology, Federal University of São Paulo (UNIFESP), São Paulo, São Paulo, Brazil

Abstract

Quantitative fundus autofluorescence (qAF) is an approach that is built on a confocal scanning laser platform and used to measure the intensity of the inherent autofluorescence of retina elicited by short-wavelength (488 nm) excitation. Being non-invasive, qAF does not interrupt tissue architecture, thus allowing for structural correlations. The spectral features, cellular origin and topographic distribution of the natural autofluorescence of the fundus indicate that it is emitted from retinaldehyde-adducts that form in photoreceptor cells and accumulate, under most conditions, in retinal pigment epithelial cells. The distributions and intensities of fundus autofluorescence deviate from normal in many retinal disorders and it is widely recognized that these changing patterns can aid in the diagnosis and monitoring of retinal disease. The standardized protocol employed by qAF involves the normalization of fundus grey levels to a fluorescent reference installed in the imaging instrument. Together with corrections for magnification and anterior media absorption, this approach facilitates comparisons with serial images and images acquired within groups of patients. Here we provide a comprehensive summary of the principles and practice of qAF and we highlight recent efforts to elucidate retinal disease processes by combining qAF with multi-modal imaging.

---

[1]Percentage of work contributed by each author in the production of the manuscript is as follows: Janet R. Sparrow: 94%, Tobias Duncker: 0.5%, Kaspar Schuerch: 0.5%, Maarjaliis Paavo: 2%, Ronaldo Carvalho: 3%.

[*]Corresponding author. Department of Ophthalmology, Columbia University, New York, NY, 10032, USA. jrs88@columbia.edu (J.R. Sparrow).

Author statement

Percentage of work contributed by each author.

Janet R Sparrow 95%,

Tobias Duncker 0.5%,

Kaspar Schuerch 0.5%,

Maarjaliis Paavo 2%

Ronaldo Carvalho 2%

Keywords

Age-related macular degeneration; ABCA4; Acute zonal occult outer retinopathy; Confocal scanning laser ophthalmoscopy; Fundus; Fundus autofluorescence; Quantitative fundus autofluorescence; Recessive stargardt disease; Retina; Retinitis pigmentosa

1. Introduction

1.1. Fundamentals of fundus autofluorescence imaging

The retina emits an intrinsic autofluorescence when excited with short-wavelength (SW) light ('blue autofluorescence') (Fig. 1A). SW fundus autofluorescence (SW-AF) can be excited *in vivo* in the spectral range between 400 and 590 nm, with a peak excitation at 490–510 nm (Delori et al., 1995a). The fluorescence is emitted at wavelengths between 520 and 800 nm with a peak at approximately 600 nm. In clinical settings this emission has been imaged as fundus autofluorescence (AF) (von Ruckmann et al., 1995; von Ruckmann et al., 1997) using confocal scanning laser ophthalmoscopy (cSLO; 488 nm excitation) (Delori et al., 2007; Holz et al., 1999) or by using a modified fundus camera (535–580 nm range) (Spaide, 2007) and more recently by ultra-wide-field ophthalmoscopic technology (200° field; 532 nm excitation) (Lengyel et al., 2015; Nagiel et al., 2016; Yung et al., 2016). The spectral characteristics and the cellular source of SW-AF in healthy eyes indicate that this natural autofluorescence originates from the family of autofluorescent bisretinoid compounds (lipofuscin) that have been isolated and characterized including A2-GPE (A2-glycerophosphoethanolamine), all-*trans*-retinal dimer, A2E and *cis* isomers of A2E, and A2-DHP-PE (A2-dihydropyridine-phosphatidylethanolamine) (Fishkin et al., 2005; Kim and Sparrow, 2018; Kim et al., 2007; Parish et al., 1998; Wu et al., 2009; Yamamoto et al., 2011). In the nomenclature used to identify bisretinoids, A2 refers to a compound that forms from 2 vitamin A-aldehyde molecules. These bisretinoid fluorophores form from irreversible non-enzymatic reactions of retinaldehyde with lipid (phosphatidylethanolamine) in photoreceptor outer segment discs. In healthy eyes these autofluorescent pigments accumulate with age in retinal pigment epithelial cells (RPE) as lipofuscin (Delori et al., 1995a; Sparrow et al., 2010a, 2010b).

In the healthy fundus, the SW-AF signal is attenuated centrally due to absorption of the incoming exciting light by macular pigment and melanin (Fig. 1A). Outside the macula, the SW-AF signal is relatively homogeneous and represents the distribution of RPE lipofuscin. Blood vessels are deficient in AF due to blockage of the SW-AF signal while the optic disk is dark due to the absence of SW-AF emission.

A second form of autofluorescence can be generated using near-infrared excitation (NIR-AF; 787 nm excitation, > 830 nm emission) (Kellner et al., 2009) (Fig. 1B). NIR-AF is considered to originate primarily from RPE melanin with a lesser contribution from choroidal melanocytes (Keilhauer and Delori, 2006; Paavo et al., 2018). In NIR-AF images, the pattern of AF is, in part, the opposite of that observed in the SW-AF images. Thus in the healthy eye, the NIR-AF signal is greatest in an area centered on the fovea and having a horizontal width of 8.8°. This area corresponds to the region in SW-AF and color fundus

images where the optical density of melanin is greatest (Keilhauer and Delori, 2006). Information gleaned from quantitation of NIR-AF intensities indicates that at elevated lipofuscin levels, as exist in *ABCA4*-disease, the lipofuscin fluorophores contribute to the NIR-AF signal (Paavo et al., 2018) (Section 7).

To quantify fundus SW-AF, some early studies of SW-fundus AF in human subjects employed noninvasive spectrophotometry to quantify AF intensities at selected positions in the fundus (Delori et al., 1995a, 1995b, 2001). This work elucidated relationships between RPE lipofuscin accumulation and age, and demonstrated increases in fundus AF in retinal disorders, such as recessive Stargardt disease. However, this approach was limited by the custom instrumentation and was appropriate to only certain retinal diseases. Other approaches using the cSLO have provided information by constructing horizontal and vertical profiles of fundus autofluorescence intensities centered on the fovea or by sampling retina in regions of predetermined pixel size (Cideciyan et al., 2004; Lois et al., 2000; Lois et al., 1999; von Ruckmann et al., 1995; von Ruckmann et al., 1997).

In this review we discuss the employment of procedures for quantifying SW-AF in fundus images acquired with a confocal laser scanning ophthalmoscope (cSLO). Quantitative fundus autofluorescence (qAF) combines measurements of AF intensity with spatial information and allows disease related changes to be distinguished from healthy age-related increases in lipofuscin. We will discuss the ways that qAF serves to establish genotype-phenotype correlations, guide clinical diagnosis and genetic testing and further our understanding of disease processes. These studies have expanded our appreciation of retinal disorders that involve changes in lipofuscin distribution and concentration. The qAF approach has broad clinical application.

2. Principles of quantitative fundus AF (qAF)

A conventional fundus AF image records the spatial distribution of the autofluorescence signal with each pixel being assigned a grey value between 0 and 255. Since in many retinal disorders the distribution of AF intensities within the fundus deviates from normal, qualitative descriptions of these changes have made important contributions to the diagnosis and monitoring of these conditions (Cideciyan et al., 1998; Fleckenstein et al., 2011; Robson et al., 2012; Solbach et al., 1997; Strauss et al., 2016). Nevertheless, with the widespread use of fundus AF in clinical settings it became apparent that additional information could become available through the development of a quantitative approach that would combine measurements of fundus AF intensity with spatial information. The qAF method that will be discussed here uses a standardized approach that employs confocal laser scanning ophthalmoscopes with a 30° × 30° field, 488 nm excitation, and emission capture from 500 to 680 nm (HRA2, Spectralis HRA + OCT, Heidelberg Engineering, Heidelberg Germany). The qAF values are calculated using a published formula (Delori et al., 2011a) that considers factors such as laser power, the laser off-set (zero signal provided by the instrument software), detector sensitivity, correction of refractive errors, and variations in anterior media structures such as the lens (Delori et al., 2011a, 2016a, 2016b).

2.1. Internal reference

The qAF approach aims to permit comparisons amongst serial images of the same subject or amongst different subjects. To this end pixels are calibrated to the greyscale values recorded in an internal autofluorescent reference mounted in the instrument (Delori et al., 2011a, 2016b) (Fig. 2A). The reference compensates for variations in sensitivity setting and laser power.

2.2. Histogram stretch

Instruments utilized to acquire conventional fundus AF images typically utilize image processing to adjust image quality by spreading image intensity values to the full greyscale range (0–255) (histogram stretching). While image contrast is substantially increased by this normalization process, grey level intensities within the images cannot be compared amongst subjects nor within serial images acquired from the same subject. Thus the qAF protocol uses cSLO images saved in the non-normalized mode (no histogram stretching).

2.3. Sensitivity setting

To ensure that the recorded signal intensity is proportional to the actual SW-AF signal emitted at the fundus the sensitivity setting of the cSLO should be adjusted to elude non-linearity due to detector saturation. Images acquired outside the dynamic range of the detector (HRA2, Spectralis HRA + OCT: grey level < 175) can underestimate (at high actual intensities) or overestimate (at very low grey levels) the true signal (Delori et al., 2011b). In the presence of high qAF levels, such as in patients with *ABCA4*-disease, relatively lower sensitivity settings are used but these should generally be maintained at a level higher than 70 so as to be within the dynamic range of the instrument.

2.4. Magnification correction

The magnification of features in a fundus image vary with the axial length/corneal curvature of a given eye (Holden and Fitzke, 1988; Rudnicka et al., 1998; Sanchez-Cano et al., 2008). For instance, the size of a feature in the image will be less for greater axial lengths (myopic eye) than for smaller axial lengths (hyperopic eye). Thus it is also essential to correct for the magnification (scaling factor) (Delori et al., 2011a) of the captured image according to the focus setting of the instrument and the corneal curvature of the subject with reference to an emmetropic eye (7.7 mm corneal curvature). The correction will be less accurate for subjects in whom refractive errors do not correlate with axial length (e.g. after corneal refractive surgery).

2.5. Ocular media

The fluorescent signal emitted at the fundus can be attenuated due to absorption of the exciting and emitted light by the lens and other anterior segment structures. This is particularly an issue with increasing age. In phakic patients without cataract, published data (van de Kraats and van Norren, 2007) have been used to adjust for the optical density of ocular media at a given age and wavelength. Correction for ocular media absorption in this way results in an increase in calculated AF. An approach enabling media correction in individual subjects will be necessary before it is feasible to make a meaningful comparison

of qAF levels in subjects with cataracts. In pseudophakic eyes, the transmission factor of a specific intraocular lens implant is included in the formula used to calculate qAF.

2.6. Macular pigment

The carotenoids lutein and zeaxanthin that constitute macular pigment have absorption spectra in the 400–540 nm range with a maximum at ~460 nm (Bone et al., 2007; Snodderly et al., 1984). The spatial distribution of macular pigment is visible in SW-AF images as a dark spot in the fovea (Figs. 1A and 2A, B) that is about 2–3° in diameter. Nonetheless, macular pigment topography can vary amongst individuals (Delori, 2004). At eccentricities of 7–8° (2–2.3 mm) absorption by macular pigment is negligible (Bone et al., 1988); thus calculation of qAF within concentric segments 7–9° eccentric to the fovea (as described below) is not affected by macular pigment absorption.

2.7. Image illumination

Uniform illumination of the fundus in SW-AF images should be achieved by careful positioning of the patient in the chin rest and is dependent on the position and orientation of the camera, and the distance between camera and cornea.

2.8. Image acquisition

To obtain high quality images, a trained and committed operator is essential. All images are acquired using a confocal laser scanning ophthalmoscope (30° × 30° field; 488 nm excitation, barrier filter transmitting light from 500 nm to 680 nm; laser power < 260 μW; HRA2 or Spectralis HRA + OCT, Heidelberg Engineering, Heidelberg, Germany). To avoid obstruction by the pupil, pupils are dilated to a minimum diameter of 7 mm (using 1% tropicamide and 2.5% phenylephrine) and the laser beam is centered on the pupil of the eye. With room lights turned off, an infrared-reflectance (NIR-R) image (820 nm) is recorded first.

After switching to the blue (488 nm) excitation mode, the image is refocused to ensure a uniform signal over the entire 30° × 30° field; the whole field should have even and maximum intensity. Since the retinaldehyde chromophore of visual pigment is densely packed in photoreceptor outer segments and is an efficient absorber of light (Morgan and Pugh, 2013), it can serve to screen the exciting and emitted light. Thus during set-up and focusing in blue excitation mode, the fundus is exposed for 20 s to reduce visual pigment absorption. Retinal light exposures used are below the maximum permissible levels recommended by the American National Standards Institute for 8 h exposure (ANSI., 2014; Delori et al., 2016b).

The detector sensitivity is adjusted so that grey levels do not exceed the linear range of the detector (grey level < 175). Each image is acquired in high-speed video mode (8.9 frames/second); two images are recorded, each being typically 9–12 frames. All video images are examined for image quality and at least 6 of the 9–12 frames are selected. Selected frames are aligned and averaged and saved in non-normalized mode. Additional aspects of the imaging protocol have been described (Burke et al., 2014; Delori et al., 2011a; Duncker et al., 2014, 2015a, 2015b, 2015c; Greenberg et al., 2013; Sparrow et al., 2016).

2.9. Image exclusion

Images should be excluded if there are appreciable media opacities, corneal opacities or visible shadows due to floaters or irregular fundus illumination. Insufficient pupillary dilation will present as generalized decreased signal while eyelash interference will manifest as localized decreased signal. Misalignment of frames due to eye movement is another reason to exclude an image. Tear film instability can also be a problem. Poor image quality is typically associated with reduced qAF values.

2.10. Image analysis

For qAF analysis, custom software written in IGOR (Wavemetrics, Lake Oswego, OR) has been used (Delori et al., 2011a), as has the HEYEX software (Heidelberg Engineering). Briefly, grey levels in the fundus image are standardized to the grey level of the internal reference (Fig. 2A) after accounting for the electronic zero grey level, sensitivity, magnification (provided by Heidelberg software) and ocular media absorption as described (Delori et al., 2011a). The software permits retinal vessels and atrophic areas to be excluded by histogram analysis. Color-coded fundus maps illustrating the distribution of qAF levels can be generated such that each pixel is assigned a color based on the associated qAF value (Fig. 2B). To obtain a single qAF value for comparative purposes, mean qAF can be computed in preset regions (Fig. 2A). For this purpose measurement areas have been standardized as three concentric rings (outer, middle, inner) divided into 8 segments in addition to a central foveal area. qAF_8 refers to the mean qAF of the eight segments in the middle ring (eccentricity, 7°–9°). For each eye, mean qAF_8 is calculated from images acquired in one or two imaging sessions. The analysis of qAF can also follow a region of interest qAF (ROI-qAF) approach using manually selected rectangular areas of the image (Boudreault et al., 2017; Schuerch et al., 2017) (Sections 4.2 and 4.5).

2.11. Repeatability

Inter-session repeatability (session 1 versus session 2; 95% confidence interval) has been calculated when second imaging sessions are performed after refocusing, realigning and resetting the detector sensitivity. The intersession Bland-Altman coefficient of repeatability has ranged from 6% to 11% (Delori et al., 2011a; Duncker et al., 2014, 2015b, 2015c). Thus qAF measurements acquired in a second session are expected to only differ from the first by more than 6–11% on 5% of occasions. For the qAF_8 of right and left eyes the Bland Altman coefficient of agreement has been 13%–19% (Burke et al., 2014; Duncker et al., 2014; Greenberg et al., 2013). Repeatability after 3 and 6 month follow-up in eyes without retinal changes has ranged from 8.3% to 9.8% (Reiter et al., 2018).

3. qAF in healthy eyes

Consistent with other approaches (Feeney-Burns et al., 1984; Kim et al., 2007; Weiter et al., 1986; Wing et al., 1978) used to measure lipofuscin accumulation in retina, qAF intensities increase with the age of the subject (Greenberg et al., 2013) (Fig. 2C). qAF is also higher for white individuals and lower for Asians and blacks (Fig. 2C). The relationship between ocular pigmentation and qAF has been confirmed in mice wherein an absence of ocular pigmentation confers higher qAF intensities (Paavo et al., 2018). qAF is also higher in

smokers and females (Greenberg et al., 2013). In the healthy eye, qAF levels are highest superotemporally (Fig. 2B) and increase with increasing eccentricity up to 10°–15° outside of the fovea (Greenberg et al., 2013).

4. qAF in human retinal disorders

4.1. Bestrophin-1 associated disease

Mutations in the gene *Bestrophin-1* (*BEST1*; 11q13) cause retinopathies (referred to here as Best vitelliform macular dystrophy, BVMD) varying in age of onset, inheritance patterns, rate of progression and presence of single versus multiple lesions. More than 200 disease-causing mutations (Johnson et al., 2017) have been described most of which are missense mutations (Johnson et al., 2017). The bestrophin-1 (BEST1) protein is localized to the basolateral plasma membrane of RPE (Johnson et al., 2017; Marmorstein et al., 2000; Petrukhin et al., 1998) and functions as an anion channel that is permeable to chloride and that is activated by changes in cytosolic calcium concentration (Gomez et al., 2013; Hartzell et al., 2008; Johnson et al., 2017; Kane Dickson et al., 2014; Milenkovic et al., 2011; Neussert et al., 2010; Qu and Hartzell, 2008; Sun et al., 2002; Tsunenari et al., 2003; Xiao et al., 2010; Yang et al., 2014; Zhang et al., 2010). A hallmark of Best vitelliform macular dystrophy is a central oval lesion that appears egg yolk-like (vitelliform lesion) in color fundus photographs and exhibits intense autofluorescence in SW-AF images (Duncker et al., 2014; Spaide et al., 2006) (Fig. 3A, B, D). The vitelliform lesion is also readily observed in NIR-AF images (Fig. 3C). In spectral domain optical coherence tomography (SD-OCT), the lesion is visible as a dome-shaped fluid-filled separation between the RPE/Bruch's membrane complex and the hyperreflective bands attributable to the interdigitation zone and ellipsoid zone of photoreceptor cells (Duncker et al., 2014; Ferrara et al., 2010; Querques et al., 2008) (Fig. 3E). Since apical-to-basal chloride transport establishes the osmotic gradient that drives trans-epithelial water movement (retina to choroid) (Gallemore et al., 1997; Singh et al., 2013; Stamer et al., 2003), the accumulation of fluid in the subretinal space in Best vitelliform macular dystrophy can be explained. The assignment of a basolateral chloride conductance to BEST1 can also account for the light peak of the electrooculogram (EOG) and its reduction in Best vitelliform macular dystrophy (Gallemore and Steinberg, 1993; Xiao et al., 2010). Moreover, the separation between RPE and photoreceptor cells that is imposed by the fluid in the domain-shaped detachment (Fig. 3E) would hamper the normal process of phagocytosis that follows the shedding of outer segment membrane by photoreceptor cells. Thus as expected, the outer segment debris accumulates subretinally.

Emission spectra recorded within the vitelliform lesions of Best vitelliform macular dystrophy patients exhibit maxima (580–620 nm) that are consistent with emission spectra of RPE lipofuscin recorded in healthy eyes (Duncker et al., 2014). Efforts to understand the source of the intense autofluorescence of the vitelliform lesion in SW-AF images has lead to the view that lipofuscin is increased retina-wide in Best vitelliform macular dystrophy (Bakall et al., 2007; Frangieh et al., 1982; O'Gorman et al., 1988; Singh et al., 2013; Spaide et al., 2006; Vedantham and Ramasamy, 2005; Weingeist et al., 1982; Zhang et al., 2011).

To determine whether the measurement of SW-AF can support this assumption we obtained qAF images from Best vitelliform macular dystrophy patients (2 independent cohorts; 30

patients) and applied the segmental analysis to calculate qAF (Duncker et al., 2014; Sparrow et al., 2016; Lima de Carvalho et al., 2019). For qAF calculation, grey levels were recorded from non-lesion areas using the middle ring of segments. In all eyes of Best vitelliform macular dystrophy patients, qAF measured outside the vitelliform lesion was not elevated relative to levels observed in healthy eyes (Fig. 4). These measurements of qAF indicate that RPE bisretinoid lipofuscin is not increased outside the vitelliform lesion in Best vitelliform macular dystrophy.

As expected however, qAF levels are considerably elevated within the lesion as compared to non-lesion retina (Fig. 3A) and are much higher than at the same fundus position in age-similar healthy eyes (Duncker et al., 2014). As discussed above, the hyperreflective material that characterizes the vitelliform lesion in SD-OCT scans (Borman et al., 2011; Duncker et al., 2014) is continuous at the lesion-edge with the interdigitation zone and ellipsoid zone; thus this material is understood to be outer segment debris. The most parsimonious explanation for the abnormal accumulation of outer segments in the fluid-filled lesion is that phagocytosis is thwarted by the separation between RPE and photoreceptor cells. Given that bisretinoid lipofuscin fluorophores are produced in photoreceptor outer segments due to aberrant reactions of retinaldehyde (Sparrow et al., 2012a), this OS material is the likely source of the AF in the vitelliform lesion. Moreover, since formation of these fluorophores does not depend on phagocytosis, these fluorophores will form even in unphagocytosed outer segments. That said, it is readily apparent that the SW-AF intensities within the lesion are considerably greater than in non-lesion fundus. Outer nuclear layer thinning within the lesion area also indicates that photoreceptor cells within the lesion have reduced viability (Duncker et al., 2014). Taken together these observations may suggest that bisretinoid formation is increased when photoreceptor cells are impaired.

4.2. Retinitis pigmentosa (RP)

Retinitis pigmentosa (RP) can be inherited as autosomal-dominant (about 30–40% of cases), autosomal-recessive (50–60%) or X-linked (5–15%) trait (Bunker et al., 1984; Hartong et al., 2006). An autosomal dominant subgroup of RP is caused in 25% of the cases by a mutation in the rhodopsin gene.

Several noninvasive imaging modalities have been utilized to observe RP progression. In SW-AF images wherein the signal originates primarily from bisretinoid lipofuscin (Delori et al., 2007), a ring or arc of high AF is often visible within the transitional zone between degenerated and intact photoreceptor cells (Bassuk et al., 2014; Greenstein et al., 2012; Lima et al., 2009, 2012; Popovic et al., 2005; Robson et al., 2008, 2011; Sujirakul et al., 2015) (Fig. 5A). The inner border of the ring delimits an area interior to the ring that exhibits normal function (Hood et al., 2011) and a preserved hyperreflective band attributable to the ellipsoid zone on SD-OCT (Duncker et al., 2013b). Across the ring visual sensitivity is generally reduced and in SD-OCT images the outer nuclear layer is thinned and the EZ is disrupted (Aizawa et al., 2010; Duncker et al., 2013b; Greenstein et al., 2012; Hood et al., 2011; Lima et al., 2009). Pronounced degeneration peripheral to the outer border of the ring is evidenced by an absence of the photoreceptor ellipsoid zone, thinning or absence of outer nuclear layer in SD-OCT scans together with hyperreflective intraretinal

foci, and profoundly reduced or non-recordable visual sensitivity. In the area adjacent to the outer border of the ring, the ellipsoid zone band is absent but RPE/Bruch's membrane is intact (Schuerch et al., 2016). Studies employing SW-AF imaging have demonstrated that the AF rings can constrict with time (Lima et al., 2012).

The high AF ring in RP is also visible with NIR-AF imaging (Duncker et al., 2013b; Kellner et al., 2009); this modality employs an excitation light of 787 nm and generates a signal primarily from RPE and choroidal melanin (Keilhauer and Delori, 2006). The location of the outer border of the ring in NIR-AF images exhibits good correspondence with the location detected by SW-AF imaging. Conversely, the inner border of the ring was found to be closer to the fovea in the NIR-AF images and corresponded to the position in SD-OCT scans where the ellipsoid zone band was at least partially intact (Duncker et al., 2013b). The hyperautofluorescent ring in RP exhibits a greater horizontal and vertical diameter, and greater ring area in SW-AF images than in NIR-AF images. However no differences have been observed in the rate of ring constriction with time when measured in SW-AF versus NIR-AF images (Jauregui et al., 2018). Moreover, choroidal vessel visibility outside the AF ring in SW-AF and NIR-AF images is indicative of reduced RPE pigmentation (Schuerch et al., 2016) likely due to a thinned RPE monolayer that has undergone proliferation, spreading and migration in response to photoreceptor cell degeneration.

SW-AF rings are dynamic. We set out to determine whether there is an actual increase in SW-AF intensity within the borders of the ring compared to corresponding areas in healthy retina, or if the increase is only apparent due to decreased SW-AF intensity in adjacent retina (Schuerch et al., 2017). In a cohort of 40 patients, we used an ROI-qAF approach applied to superior, temporal and inferior aspects of the ring (Fig. 5) and found that for 28% of measurements, ROI-qAF measurements within the ring were higher than at the corresponding positions in healthy retina. Even for ROI-qAF measurements acquired external to the ring, 21% of values were higher than in healthy eyes. RP patients in the RP cohort differed in terms of age and genotype and presented at various stages of the disease. Thus it is reasonable to conjecture that most AF rings at some stage of the disease would reflect an actual increase in fluorophore deposition.

What accounts for the elevated SW-AF signal? Since the AF signal generated at the position of rings in RP remains visible after bleaching of photopigment, unmasking of RPE SW-AF cannot account for the presence of the rings (Schuerch et al., 2017). A window defect created by degenerated photoreceptors and allowing for an increase in the signal recorded from RPE, is unlikely to be the explanation for these AF rings. If thinning of the neural retina overlying the ring with creation of a window-defect could account for the SW-AF rings in RP, one would expect AF within the ring to be consistently higher in all RP eyes but this was not the case. Moreover, in SD-OCT images of our patient cohort, increased signal transmission into the choroid was observed at locations external to the ring, but not within the ring. Nor is the abnormal AF from the ring likely to be derived from accelerated phagocytosis of photoreceptor outer segments (Aizawa et al., 2010; Lima et al., 2012; Robson et al., 2006); the rate of bisretinoid fluorophore formation is predetermined in photoreceptors. That is, bisretinoids form before outer segment shedding and subsequent

phagocytosis. Instead it is likely that the AF rings reflect an increase in fluorophore deposition.

Since functional and structural studies indicate that photoreceptor cells within the ring are degenerating, we surmise that the process of photoreceptor cell degeneration leads to an increase in the bisretinoid lipofuscin fluorophores that are the source of SW-AF. There is considerable evidence (Sparrow et al., 2012a) that bisretinoids are light sensitive compounds that photogenerate reactive oxygen species and photodecompose into dicarbonyl-(glyoxal, GO; methylglyoxal, MG) and aldehyde-bearing fragments (Wu et al., 2010; Yoon et al., 2012) that damage proteins and other macromolecules. An increase in bisretinoid formation as a secondary feature of the disease process may explain why light has been shown to accentuate disease processes in several animal models of RP (Budzynski et al., 2010; Iwabe et al., 2016; Naash et al., 1996; van Wyk et al., 2015; Vaughan et al., 2003; White et al., 2007).

4.3. Recessive stargardt disease (STGD1)

Disease-related variants in *ABCA4* are the most common cause of juvenile macular degeneration (Fishman et al., 1987). Visual symptoms typically occur in the second decade of life but onset can also be earlier and loss of central vision is progressive. The *ABCA4* gene encodes a protein by the same name (originally rim protein (Papermaster et al., 1978) that is required to remove *N*-retinylidene-phosphatidylethanolamine (NRPE), formed by the binding of retinaldehyde to phosphatidylethanolamine (PE), from the photoreceptor outer segment disc membranes. Unusual inefficiency in this process, such as occurs in STGD1 due to mutations in *ABCA4*, accelerates the reactivity of NRPE with a second molecule of retinaldehyde, leading to the irreversible formation of bisretinoids (Sun and Nathans, 2001; Weng et al., 1999). Histopathological studies of eyes from patients with STGD1 (Birnbach et al., 1994; Eagle et al., 1980; McDonnell et al., 1986; Steinmetz et al., 1991), spectrophotometric analysis of fundus AF (7° temporal to the fovea; 510 nm excitation) (Delori et al., 1995b), and assessment of images acquired by cSLO (Cideciyan et al., 2005; Lois et al., 2000, 2004) have shown that RPE bisretinoid lipofuscin is considerably higher in STGD1 patients than in control age similar subjects. Additionally, *Abca4* null mutant mice exhibit elevated bisretinoid lipofuscin, measured chromatographically and by SW-AF (measured as qAF) (Kim et al., 2004; Maeda et al., 2009; Sparrow et al., 2013; Weng et al., 1999). We sought to determine whether the qAF approach that includes normalization to an internal autofluorescent reference along with corrections for magnification and optical media density would facilitate inter-patient comparison in genetically confirmed cases of *ABCA4*-associated disease.

As expected, *ABCA4* mutations in a cohort of 42 patients were found to be associated with elevated qAF (Burke et al., 2014) (Fig. 6A). In the case of some young patients, levels could be up to 8-fold higher than in healthy eyes (Fig. 6A, C). The high degree of interocular symmetry observed in STGD1 includes qAF (Fig. 6B). The spatial distribution of fundus autofluorescence in the STGD1 patients was similar to that in healthy eyes; qAF intensities were highest in the supero-temporal quadrant and lowest in the infero-nasal quadrant (Fig. 6D). While qAF increased with age in healthy controls, for STGD1 patients no association

with age was noted. Indeed, the decrease with age observed in the presence of some *ABCA4* variants (Fig. 6A) is likely attributable to photobleaching of the bisretinoid fluorophores and loss of RPE cells (Ben-Shabat et al., 2002; Jang et al., 2005; Kim et al., 2006, 2008, 2010; Liu et al., 2015; Sparrow et al., 2002, 2003a, 2003b; Ueda et al., 2016; Wu et al., 2010, 2014; Yamamoto et al., 2012; Yoon et al., 2011; Zhao et al., 2018; Zhou et al., 2005). Not surprisingly, the highest qAF values were observed for eyes with numerous hyperautofluorescent flecks (Fig. 9A) (flecks are discussed in Section 4.3.4). Conversely, when darkened flecks and atrophy were observed within the analyzed segments (7–9° eccentricity) qAF was decreased.

4.3.1. Genotype-phenotypes in ABCA4-disease—Establishing genotype-phenotype correlations in *ABCA4*-related disease is challenging because of the large number of known disease-causing mutations (at least 800 within the coding and non-coding regions) in the *ABCA4* gene (OMIM 601691, NM_000350.2) and because of the frequency of compound heterozygosity. In STGD1 patients carrying the disease-causing *ABCA4* mutations p. L2027F and p.[L541P; A1038V], qAF was higher while p. A1038V (when not in conjunction with p. L541P), p. G851D, and p. G1961E were associated with qAF levels that were lower than observed with other mutations [Burke et al., 2014 #3611]. The complex allele p.[L541P; A1038V] results in protein misfolding and imparts rapidly elevating qAF and thus a severe phenotype resulting in early disease onset and relatively faster disease progression (Cideciyan et al., 2009). The analysis by qAF and these clinical findings are consistent with *in vitro* ABCA4 activity assays showing that the p. L541P mutation alone or in combination with p. A1038V (p.[L541P; A1038V] complex allele) is associated with impaired basal and all-*trans*-retinal stimulated ATPase activity (Sun et al., 2000; Zhang et al., 2015). Moreover, a mutant mouse homozygous for a dual knock-in of the complex allele (*Abca4*$^{PV/PV}$) expressed profoundly reduced levels of Abca4 protein due to degradation of misfolded protein, and substantial levels of bisretinoid lipofuscin (Sun et al., 2000; Zhang et al., 2015). The missense mutation p. P1380L was also associated with elevated qAF compared to other mutations in the cohort. This mutation is considered severe and is suggested to cause either impaired ATP binding or altered transport of ABCA4 protein (Cideciyan et al., 2009; Sun et al., 2000). When p. P1380L is carried as a homozygous mutation (Fig. 6D) or as a compound heterozygous mutation with p. R2030Q or IVS40+5G > A, the mutation is associated with central atrophy and widespread disease (Hwang et al., 2009) while if it is harbored in compound heterozygosity with p. R2077W, autosomal recessive cone-rod dystrophy results (Kitiratschky et al., 2008).

The missense mutation p. G1961E is the most common disease causing allele and is of interest since the clinical features associated with the mutation are typically confined to an atrophic-appearing foveal lesion (bull's eye phenotype) (Fig. 6D). The absence of retina-wide disease in association with the p. G1961E allele is consistent with qAF being lower (measured 7–9° outside the fovea) than with other mutations; indeed, in some cases qAF in the presence of the p. G1961E allele is within normal limits (Fig. 6D).

qAF has also been helpful in deciphering the contribution to disease made by some *ABCA4* variants. For instance, the intronic variant c.8599T > C is predicted to affect splice-site signals and depending on the pairing of this variant with the second mutant allele, the

phenotype can vary from mild to severe (Lee et al., 2017). Information from *in vitro* ABCA4 activity assays to corroborate the effect of the variant, is not available. However, analysis of qAF revealed that c.859–9T > C can confer high lipofuscin levels (above the 95% confidence interval for healthy eyes) even at relatively young ages (Lee et al., 2017). Patients affected by a severe rapid-onset chorioretinopathy phenotype of *ABCA4*-disease were observed to harbor deleterious null biallelic *ABCA4* mutations (Tanaka et al., 2018). Levels of qAF in the macula were not only higher than the 95% confidence intervals of healthy eyes but were also higher than in other patients diagnosed with *ABCA4*disease. Disease in the macula began with intense autofluorescence in SW-AF images which progressed to an attenuated NIR-AF signal indicative of advanced disease in RPE and photoreceptor cells.

The clinical presentation of *ABCA4* disease can vary with the spectrum of phenotypes including bull's eye maculopathy, cone-rod dystrophy and severe RP (Bertelsen et al., 2014; Cella et al., 2009; Cremers et al., 1998; Duncker et al., 2015b; Martinez-Mir et al., 1998; Maugeri et al., 2000). Amongst patients carrying *ABCA4* mutations we have noted individuals presenting with a rapid-onset chorioretinopathy. A 10 year old patient that harbored mutation (c.5312+1G > A and p. R2030) conferring null alleles, is representative of this group. qAF measured in this child was higher than in healthy eyes and higher and at a younger age than in other STGD1 patients not exhibiting this phenotype (> 1000 qAF units in both eyes) (Tanaka et al., 2018). Distinctive in this group of patients was generalized SW-AF brightness in the macula that corresponded spatially to attenuated NIR-AF.

4.3.2. qAF and bull's eye phenotype in ABCA4-disease—One challenge to the diagnosis of inherited retinal dystrophies is that mutations in different genes can be associated with similar phenotypes. For instance patients having *ABCA4*-associated disease, can present with a variety of different phenotypes one of which is a bull's eye maculopathy. Moreover, a bull's eye phenotype can be associated not only with *ABCA4* disease but also mutations in other photoreceptor-associated genes such as RPGR (retinitis pigmentosa GTPase regulator) and PROM1 (Prominin 1). Thus there are challenges inherent in the use of conventional fundus AF images to discriminate amongst patients who may or may not carrying *ABCA4* mutations. In a cohort of patients exhibiting a bull's eye-like phenotype (37 patients) we set out to determine whether qAF can make this distinction (Duncker et al., 2015b) (Fig. 7). We defined the bull's eye phenotype as a localized macular lesion exhibiting a smooth contour with a parafoveal ring of increased SW-AF and a normal appearing extra-macular fundus without flecks (Fig. 7A and B). In these patients the ring of increased autofluorescence that surrounded the hypoautofluorescent lesion correlated in all eyes with the outer limits of a central area of ellipsoid zone discontinuity or loss (Fig. 7C). Whereas qualitative features of fundus autofluorescence and SD-OCT images did not serve to distinguish *ABCA4*-positive versus *ABCA4*-negative patients, *ABCA4*-positive patients (Fig. 7D, red and blue symbols) having a bull's eye phenotype had higher qAF levels, measured at an eccentricity of 7–9° (Fig. 7B, D, E; F red symbols), than the range in healthy subjects (Fig. 7F, black solid and dashed lines). These patients also tended to have higher qAF values than *ABCA4*-negative patients (Fig. 7F, black symbols) (Duncker et al., 2015b). Indeed, in the *ABCA4*-negative group, 22/26 eyes (13/15 patients) exhibited *qAF* within the normal range. The *ABCA4*-positive patients also clustered at younger ages than the

ABCA4-negative patients (Fig. 7F, blue and red symbols versus black symbols). Of the two *ABCA4*-positive patients that had qAF_8 within the normal range for their age, one was homozygous and the other one heterozygous for p. G1961E (Duncker et al., 2015b) (Fig. 7F, blue symbols). Thus qAF levels within the normal range do not eliminate the likelihood of *ABCA4* mutations but they substantially increase the odds of finding causal mutations in genes other than *ABCA4*.

4.3.3. qAF and a pattern dystrophy phenotype—*ABCA4*-mutations can present with a pattern dystrophy phenotype similar to that associated with mutations in *PRPH2/RDS*-associated disease. This phenotype is often characterized by a butterfly-shaped lesion in the macula that includes central mottling or atrophy with peripapillary sparing and perhaps foveal sparing, and flecks (Boon et al., 2007; Marmor and McNamara, 1996; Renner et al., 2009; Watzke et al., 1982). We studied a cohort of 39 patients exhibiting pattern dystrophy. The sub-set of patients with pattern dystrophy-like *ABCA4*-related disease typically, but not always, expressed higher qAF levels than healthy eyes (Fig. 8). Moreover, in some cases the *PRPH2/RDS*-positive individuals had higher qAF than healthy eyes while generally having lower qAF than the group of patients with pattern dystrophy-like *ABCA4*-related disease. The group of pattern dystrophy patients without mutations in *ABCA4* or *PRPH2/RDS* had qAF that was not different from the normal range for age (Duncker et al., 2015c).

4.3.4. Fundus flecks in ABCA4-associated disease—Autofluorescent fundus flecks are conspicuous features of fundus autofluorescence images acquired from patients presenting with STGD1. In color-coded qAF images in which colors are assigned to each pixel based on qAF values scaled to a range of 0–1200, flecks exhibit levels of qAF that are 1.5 to 2-fold greater than neighbouring fundus (Paavo et al., 2019) (Fig. 9A).

Hyperautofluorescent flecks in SW-AF images typically co-localize with larger darkened foci in NIR-AF images; the latter presentation is indicative a loss of RPE cells (Paavo et al., 2019; Sparrow et al., 2015) (Fig. 9B and C). With time the bright autofluorescence of flecks is also extinguished (Fig. 10). In SD-OCT images, flecks correspond to hyperreflective deposits in photoreceptor-attributable bands indicative of ongoing photoreceptor cell degeneration. These findings indicate that the bright SW-AF signal of flecks originates, not from RPE cells as assumed (Eagle et al., 1980; Lopez et al., 1990), but from augmented lipofuscin formation in degenerating photoreceptor cells impaired by RPE failure/loss. These findings have lead us to suggest that flecks in STGD1 are a manifestation of groups of photoreceptor cells degenerating after the loss of RPE. The elevated production of bisretinoid reflected in the increased SW-AF signal could accelerate photoreceptor cell degeneration and contribute to the natural history of STGD1.

4.3.5. qAF is not increased in carriers of ABCA4 mutations—In heterozygous carriers of *ABCA4* mutations, qAF and outer retinal thickness (SD-OCT) were within 95% confidence intervals for healthy non-carrier eyes; *ABCA4*-affected family members had elevated qAF. Perifoveal fleck-like fundus abnormalities were observed in 4 carriers (Duncker et al., 2015a). In heterozygous carriers of *ABCA4* mutations (75 subjects), qAF levels were not elevated relative to healthy non-carrier individuals. In a small sub-group of

carriers perifoveal fleck like changes were observed. Similar findings were generated in a second study of individuals carrying monoallelic *ABCA4* mutations (Muller et al., 2015). Here qAF measurements acquired from heterozygous carriers of an *ABCA4* mutation were not different than measurements from age-matched controls. This was the same for missense and truncating mutations (Muller et al., 2015). Thus carrier status associated with approximately half of the ABCA4 protein content does not confer elevated SW-AF indicative of increased RPE lipofuscin.

4.4. Age related macular degeneration (AMD)

Gliem and colleagues have measured qAF in early and intermediate age-relative macular degeneration (Gliem et al., 2016). While the investigators expected lipofuscin/qAF levels to be elevated in AMD, they found that qAF measurements in patients with soft and cuticular drusen were within 95% confidence intervals of qAF values in age-adjusted control healthy eyes. In patients with reticular pseudodrusen, qAF levels were below the 95% confidence intervals. As suggested by the authors, reduced lipofuscin in AMD could reflect reduced rod and cone densities or slowing of the visual cycle. Given that it is well known now that the bisretinoid fluorophores that constitute RPE lipofuscin undergo damaging photodegradation processes (Ueda et al., 2016), normal levels or reduced qAF in AMD is likely to be a sign of cellular injury contributing to disease processes.

4.5. Acute zonal occult outer retinopathy (AZOOR)

The etiology of AZOOR, an uncommon disease, is poorly understood and the early clinical recognition of AZOOR can be challenging (Fekrat et al., 2000; Fine et al., 2009; Jung et al., 2014; Mrejen et al., 2014). Central visual acuity in these patients can be good due to foveal sparing. Recent efforts to define the fundus features of AZOOR have relied on the presence of a lesion that surrounds the optic nerve and presents in SW-AF images as hypoautofluorescence indicative of RPE atrophy. The border between lesion and non-lesion retina is often demarcated by a conspicuous hyperautofluorescent (AF) line (AZOOR line); the AZOOR line marks a precipitous change from normal to decreased or nonrecordable visual sensitivities recorded by fundus perimetry (Duncker et al., 2018b; Fekrat et al., 2000; Mrejen et al., 2014). The lesions in SW-AF images correspond to disruptions of the ellipsoid and interdigitation zones of the photoreceptor cell attributable bands in OCT scans together with outer nuclear layer thinning and hypertransmission into the choroid indicative of RPE/Bruch's involvement (Duncker et al., 2018a; Mrejen et al., 2014). While AZOOR lesions typically include peripapillary involvement with centrifugal progression, less frequently patients present with peripheral concentric zonal atrophy that progresses centripetally (Tan et al., 2017). The underlying pathologic process, either autoimmune, infectious, or inflammatory, triggering the development of AZOOR is still under debate (Jampol and Becker, 2003) but the disease is considered to involve photoreceptor cells, RPE and choroid (Jung et al., 2014; Mrejen et al., 2014).

Early diagnosis depends on advances in imaging modalities that can improve phenotyping and contribute to an understanding of the underlying pathogenesis. To further elucidate the disease process we utilized qAF to objectively measure SW-AF intensities in AZOOR (Boudreault et al., 2017) and compare these intensities to healthy eyes over time (Burke et

al., 2014; Duncker et al., 2014). As noted above, increased autofluorescence, relative to other fundus areas, is observed at the junction of diseased versus non-diseased retina but whether the fluorescence is actually increased relative to healthy eyes was a question we wanted to address. In 3 of 5 patients in whom ROI-qAF intensities were measured on the AZOOR line, ROI-qAF levels within the border were significantly elevated relative to the same fundus position in healthy eyes (Boudreault et al., 2017). Since in one of these patients, ROI-qAF levels returned to normal when re-measured after 6 years, the two additional patients not presenting with elevated ROI-qAF may have exhibited higher autofluorescence levels, at the border between diseased and non-diseased retina, at an earlier stage of the disease.

The finding that qAF is elevated on the AZOOR line indicates that the process of photoreceptor cell degeneration may involve increased bisretinoid formation. Analysis of SD-OCT scans through the ROI positions on the AZOOR line revealed disruptions of outer retinal reflectivity layers at the positions of elevated qAF. Retinal pigment epithelium (RPE) atrophy was indicated either by thinning of the Bruch's membrane/RPE reflectivity layer or increased transmission of signal into the choroid. Photoreceptor cell degeneration was evidenced by ellipsoid zone disruption and outer nuclear layer thinning. On the other hand ROI-qAF nasal and temporal to the border was profoundly reduced relative to the same fundus location in the healthy control group. To test for a more widespread change in SW-AF we also measured qAF within the 8-scaled segments positioned over healthy non-diseased areas of affected eyes; qAF levels were within the normal range as indicated by the mean and 95% confidence intervals of healthy age-and ethnicity-matched eyes.

A window-defect created by the loss of outer retinal layers and allowing for increased AF signal from RPE is unlikely to account for the increased SW-AF within the AZOOR line since in SD-OCT scans at this location the RPE/Bruch's reflectivity layer is also not intact. Nor can the AZOOR line be attributed to accelerated phagocytosis of photoreceptor outer segments: bisretinoid fluorophores form in photoreceptor outer segments before phagocytosis.

It has been proposed that photoreceptor cell impairment can lead to ineffective handling of reactive retinaldehyde that is generated by photoisomerization of visual pigment. Unchecked reactions of vitamin A aldehyde result in excessive production of bisretinoid fluorophores in photoreceptor cells (Sparrow et al., 2012b). The high qAF levels measured at the border of growing AZOOR lesions are consistent with this model. Since bisretinoids are phototoxic, excessive bisretinoid production could advance photoreceptor cell damage (Ueda et al., 2016). Indeed since patients with borders delineated by an AZOOR line at presentation showed more frequent progression over time (Mrejen et al., 2014), accelerated formation of lipofuscin at the transition zone may be critical in the disease process. Determination of ROI-qAF levels in a longitudinal study of a larger cohort could provide insight into these trends.

4.6. Pseudoxanthoma elasticum (PXE)

PXE is an inherited disease caused by mutations in the *ABCC6* gene (Gliem et al., 2017) and characterized by mineralization of elastic fibers in tissues such as skin, vascular tissue

and Bruch's membrane. In the eye, PXE-changes are associated with RPE and outer retina (Gliem et al., 2017). In individuals with PXE confirmed genetically or by skin biopsy, qAF values were acquired within a circular ring of segments centered at an eccentricity of 7°–9° outside the fovea (Gliem et al., 2017). When adjusted for age qAF was reduced in PXE patients relative to control healthy eyes. The difference was typically greater in older patients and the fundus distribution of qAF values revealed changes that were lower in nasal areas. Significantly, Bruch's membrane changes in PXE patients are also considered to be most severe in the nasal sector. One explanation for the reduced qAF even in patients younger than age 40 and without evidence of atrophy, could be decreased availability of vitamin A.

5. qAF is attenuated by RPE melanin

X-linked *GPR143/OA1* is the most common form of human ocular albinism. Random X-inactivation of the *GPR143/OA1* gene in RPE cells of female carriers of *GPR143/OA1* mutations causes melanin pigmentation in the posterior pole to acquire a mosaic pattern. In a retrospective analysis of NIR-AF images acquired from 5 *GPR143/OA1* carriers, the non-uniform fundus pigmentation presented centrally as patches of brightness (melanin pigment) that alternated with patches of darkness (melanin-deficient) (Paavo et al., 2018) (Fig. 11A). Patterns in the SW-AF fundus images of *GPR143/OA1* carriers were the reverse of the patterns in NIR-AF images (Fig. 11B) with SW-AF (measured as qAF) being elevated in the melanin-deficient units of the mosaic and not elevated in the pigmented patches. These observations indicate that ocular melanin attenuates the SW-AF signal and explains why *GPR143/ OA1* carriers are readily identified in SW-AF images.

6. qAF in the mouse

Using the Spectralis (HRA + SD-OCT) we have also extended the qAF approach to mice. In these preclinical studies using mouse models, a standardized approach allows SW-AF to be reliably measured in both wild-type and mutant mice. As compared to HPLC measurements, qAF is more efficiently measured and fewer mice are required.

6.1. Image acquisition in the mouse

The mouse eye has a relatively large numerical aperture (0.49 for a 2 mm pupil versus 0.18 for a 6 mm pupil in a human) and the lens is almost spherical (Geng et al., 2011). Thus we use a 55° lens and modified laser beam diameter and detection pupil (Sparrow et al., 2013). To prevent cataract formation due to drying of the corneal surface while the mouse is under anesthesia, a lubricant (GenTeal Liquid Gel, Novartis, East Hanover NJ) is applied topically to both corneas of the mouse and a custom made contact lens is placed on the opposite eye during imaging. Pupils are dilated to a diameter of approximately 2.5 mm by instilling 1% tropicamide and 2.5% phenylephrine. In the near-infrared reflectance mode the camera positioning and focusing is carried out; laser power is adjusted to approximately 280 μW, sensitivity to 95–100 and after switching to AF mode (488 nm), the retina is preexposed for 20 s to bleach visual pigment. Nine successive frames are then acquired with the high-speed mode (8.9 images/s). The frames were aligned and averaged and saved in the non-normalized mode to generate the qAF image for analysis.

6.2. Image analysis in the mouse

Mean grey levels are determined within 8 predefined segments located between 8.25° and 19.25° from the center of the optic disc (Fig. 12 A) and to calculate qAF, the mean grey level is calibrated to the reference after subtraction of zero light (provided by the system). In the mice qAF values are based on the means of at least 2 images obtained from the first eye recorded to minimize the likelihood that cataract formation would affect qAF results. Other details have been published (Sparrow et al., 2013).

Intersession coefficient of repeatability calculated in mice from two imaging sessions (with the camera and mouse being moved and realigned between sessions) was greater in the mice (Bland-Altman coefficient of repeatability, ± 18.6%) than that obtained for human subjects (± 6%–11%). One difference between the human and mouse studies is that focusing in the mouse is more difficult.

6.3. qAF in Abca4$^{-/-}$ and rdh8$^{-/-}$/abca4$^{-/-}$ mice

In albino *Abca4*$^{-/-}$, *Abca4*$^{+/-}$ and wild-type mice we and others have observed an age-related increase in qAF together with a chromatographically measured increase in bisretinoid (Charbel Issa et al., 2013; Flynn et al., 2014; Kim et al., 2004; Sparrow et al., 2013; Weng et al., 1999). Consistent with the known accelerated accumulation of bisretinoid as a result of ABCA4 deficiency (Kim et al., 2007; Maeda et al., 2008; Sparrow et al., 2013; Weng et al., 1999; Yamamoto et al., 2011) qAF intensities were also 1.8–2.6-fold greater in *Abca4*$^{-/-}$ versus *Abca4*$^{+/+}$ (Fig. 12B, C, E). Comparison of the rates of increase in qAF from 2 to 8 months of age as calculated by linear regression demonstrated that the slope was significantly greater for the *Abca4*$^{-/-}$ mice indicating a faster rate of increase in the latter mice relative to *Abca4*$^{+/+}$ (Sparrow et al., 2013). The change in bisretinoid levels measured as A2E (Section 1.1) was also steeper in *Abca4*$^{-/-}$ mice. We noted that the difference in A2E levels in *Abca4*$^{-/-}$ mice versus *Abca4*$^{+/+}$ mice was greater than the qAF difference (1.8–2.6-fold) (Sparrow et al., 2013). This difference could be explained by factors such as other bisretinoid fluorophores that are detected by qAF or by absorption of the qAF signal within the RPE during *in vivo* recording.

In double knock-out *Rdh8*$^{-/-}$/*Abca4*$^{-/-}$ mice qAF increased at an even faster rate than in *Abca4*$^{-/-}$ mice (Flynn et al., 2014) as expected from the absence of Rdh8 (retinol dehydrogenase 8) (Maeda et al., 2008). In these mice chromatographically measured A2E peaked at 4 months of age and then began to decline concurrent with outer nuclear layer thinning. Conversely, qAF levels in the *Rdh8*$^{-/-}$/*Abca4*$^{-/-}$ mice continued to rise between ages 4–9 months. While this difference between bisretinoid measurement and qAF is not fully understood, because this increase coincided with outer nuclear layer thinning, which is indicative of declining photoreceptor cell function and survival, elevated fundus AF due to augmented formation of bisretinoid fluorophores other than A2E could account for the continued increase in qAF.

6.4. qAF in heterozygous Abca4$^{+/-}$ mice

Despite the finding that human carriers of *ABCA4* mutations do not exhibit elevated qAF, two studies have shown that mice carrying a null mutation in *Abca4* on one chromosome

(*Abca4*$^{+/-}$), exhibit elevated bisretinoid as measured chromatographically (Charbel Issa et al., 2013; Sparrow et al., 2013). In one of these studies, qAF in the heterozygous *Abca4* mice was also consistently greater by approximately 20% although this difference did not reach statistical significance. It is notable however that since qAF in *Abca4*$^{+/-}$ mice was more similar to wild-type than to *Abca4*$^{-/-}$ mice, this finding could indicate that with one-half of the gene dosage, ABCA4 protein expression is sufficient to prevent substantially increased bisretinoid formation.

6.5. Modulation of qAF by Rpe65 in mice

In contrast to the abundant RPE lipofuscin formation associated with ABCA4 deficiency, *RPE65* mutation, as a cause of Leber congenital amaurosis, is associated with an absence or pronounced decrease in RPE lipofuscin detected by SW-AF imaging (Lorenz et al., 2004). This profound change in bisretinoid lipofuscin formation is a result of the failure to produce 11-*cis*-retinal in the absence of RPE65 activity (Jin et al., 2005; Moiseyev et al., 2005; Redmond et al., 2005). Accordingly, knock-out of the *Rpe65* gene in mice leads to an absence or pronounced decrease in RPE lipofuscin (Katz and Redmond, 2001; Wu et al., 2014), qAF values are negligible and SW-AF images have a uniformly homogeneous appearance (Zhao et al., 2017) (Fig. 12D and E).

Even a change in Rpe65 activity can modify bisretinoid production. In C57BL/6J mice an *Rpe65* polymorphism exists whereby the amino acid at residue 450 (*Rpe65*-Leu450Met) is methionine instead of leucine. This amino acid change slows the visual cycle because of reduced levels of Rpe65 protein in mouse RPE (Lyubarsky et al., 2005; Nusinowitz et al., 2003). Consequently, bisretinoid accumulation is reduced (Kim et al., 2004) and qAF is lower in the C57BL/6J^{c2j} mice (Fig. 12F). As a consequence of the decrease in bisretinoid levels, photoreceptor cells of the mice bearing the *Rpe65*-Leu450Met variant are less susceptible to light damage (Danciger et al., 2000; Wenzel et al., 2001, 2003).

6.6. qAF in mice: a measure of treatments targeting bisretinoids

Since we have shown that bisretinoid fluorophores undergo photodegradation we have hypothesized that the qAF at a given time is the product of the ratio of fluorophore synthesis in photoreceptor cells versus fluorophore photobleaching in RPE. Moreover, since the products of bisretinoid photodegradation are damaging, it is possible that the lipofuscin lost by photooxidation-associated photodegradation is more significant than the lipofuscin remaining in the cells. We tested this premise in albino *Abca4*$^{-/-}$ mice receiving a diet supplemented with the antioxidant vitamin E (Fig. 13) (Ueda et al., 2016). We observed higher levels of qAF in the treated mice (Fig. 13A) and correspondingly, higher RPE bisretinoids were evidenced by HPLC analysis (Fig. 13B). This effect was consistent with photooxidative processes known to precede bisretinoid degradation. Amelioration of outer nuclear layer thinning in the *Abca4*$^{-/-}$ mice indicated that vitamin E treatment protected photoreceptor cells (Fig. 13C) (Ueda et al., 2016).

An increase in qAF was also observed in mice treated with the iron chelator deferiprone (DFP) that reduces intracellular iron levels, thereby abating bisretinoid loss due to oxidative

degradation (Ueda et al., 2018). As with vitamin E, by decreasing the damaging effects of bisretinoid degradation, photoreceptor cell survival was promoted (Ueda et al., 2018).

6.7. qAF in the mouse is attenuated by RPE melanin

As in the studies of human albino fundus (Section 5), comparison of qAF in black C57BL/6J mice versus albino C57BL/6J-^{c2j} mice confirmed that melanin attenuated the SW-AF signal. Specifically, levels of qAF in the SW-AF images were similar in black C57BL/6J mice and albino C57BL/6J-^{c2j} mice even though we observed by chromatographic quantification that the bisretinoid A2E is lower in the albino eye due to greater photodegradation of bisretinoid. Thus the SW-AF in the albino is attributable, in part, to the greater irradiance received by the RPE fluorophores in the eyes lacking melanin (Paavo et al., 2018).

7. Interactions between SW-AF and NIR-AF intensities

The high foveal NIR-AF signal that corresponds to elevated melanin optical density in central RPE (Cideciyan et al., 2007; Keilhauer and Delori, 2006; Kellner et al., 2010; Weiter et al., 1986) suggests that NIR-AF takes its origin from melanin. Corroborating evidence to support RPE melanin as the major source of NIR-AF is provided by the NIR-AF emission associated with melanocytic choroidal nevi (Keilhauer and Delori, 2006; Kellner et al., 2010), RPE melanosomes (Gibbs et al., 2009), cutaneous melanin (Huang and Zeng, 2006) and the pigmented epithelium of the iris (Keilhauer and Delori, 2006), together with the window-defect created by a full thickness macular hole (Keilhauer and Delori, 2006). Other interpretations are not as clear. For instance, a demarcation line that is visible inferior to the optic disk in SW-AF images of even healthy eyes (Duncker et al., 2012) only becomes detectable in NIR-AF images when SW-AF/lipofuscin is elevated, as in STGD1 (Duncker et al., 2013a).

We quantified NIR-AF as grey levels along a horizontal axis through the fovea using non-normalized fundus images of STGD1 patients and healthy subjects. In patients diagnosed with *ABCA4*-associated disease, NIR-AF was increased by as much as 3-fold in tandem with increased qAF originating in bisretinoid lipofuscin. Similarly, in agouti $Abca4^{-/-}$ mice having increased SW-AF, NIR-AF was more pronounced than in wild-type mice. Moreover, the NIR-AF signal in the agouti $Abca4^{-/-}$ mice having elevated RPE lipofuscin (increased SW-AF) was greater than in agouti $Abca4^{+/+}$ mice on the same genetic background. We next examined for NIR-AF signal in the absence of melanin by studying albino $Abca4^{-/-}$ mice. As expected, NIR-AF was more pronounced in the melanin-containing (agouti) $Abca4^{-/-}$ mice than in the albino $Abca4^{-/-}$ mice. Despite the absence of melanin, the NIR-AF signal in the albino $Abca4^{-/-}$ mice increased in tandem with the age-associated increase in the SW-AF signal.

We have also compared NIR-AF image intensities in agouti $Abca4^{-/-}$ and $Abca4^{+/+}$ mice by measuring grey level in images acquired with 787 nm excitation and a sensitivity of 105; the images were saved in non-normalized mode. In the agouti $Abca4^{+/+}$ mice the NIR-AF emission is detected as expected for pigmented RPE and choroid. Interestingly however, in the agouti $Abca4^{-/-}$ mice that serve as a model of accelerated lipofuscin (elevated qAF) the NIR-AF signal was also elevated relative to the $Abca4^{+/+}$ mice. Plotting NIR-AF on the y-

axis and SW-AF on the x-axis for both agouti *Abca4*$^{-/-}$ and *Abca4*$^{+/+}$ mice revealed different slopes with the greater change in qAF (SW-AF) in the *Abca4*$^{-/-}$ mice being matched by a greater change in NIR-AF intensity. These findings indicate that bisretinoid lipofuscin, when present at sufficient concentrations, contributes to the NIR-AF signal.

8. Future directions and conclusions

The qAF approach has, at this time, not been widely incorporated into clinical routines probably because of limitations that include the requirement of a trained and committed operator, the installment of an appropriate internal fluorescent reference and software availability. Nonetheless, studies of qAF have expanded our appreciation of retinal disorders that involve changes in lipofuscin distribution and concentration. Even in our cohort of healthy eyes, there is a considerable range of qAF values and this normal range expands with age (Fig. 2C). This is an issue that will be important to better understand.

Improved awareness of genotype–qAF correlations in STGD1 and how this relationship determines other aspects of disease phenotypes is also needed. In STGD1, elevated qAF is an early feature of the natural history of disease. Nevertheless, we now know that in other retinal disorders such as retinitis pigmentosa and AZOOR, elevated qAF can be a secondary effect of the disease process especially at the advancing front of photoreceptor cell degeneration. These observations are critical since bisretinoids that are the source of SW-AF are not just markers of underlying retinal disease, they can also mediate effects of light on retinal disease. For instance the progression of retinal degeneration in some forms of retinitis pigmentosa can be aggravated by light exposure (Cideciyan et al., 1998). qAF levels that we measure reflect the balance between bisretinoid lipofuscin fluorophore synthesis in photoreceptor cells versus photooxidative loss. Since the products of the photoxidative degradation of bisretinoid are injurious to cells, it is likely that the bisretinoid lost by these processes is more significant than the lipofuscin remaining in the cells. This is an area of active investigation. We also expect that qAF can be used to reflect the activity of the visual cycle under numerous conditions. qAF will continue to increase our understanding of disease mechanisms, can serve as a biomarker of disease risk and disease progression and could have utility in the assessment of therapeutic efficacy in clinical trials.

Acknowledgements

This work was supported by National Institutes of Health grants EY024091 (JRS) and P30EY019007 and a grant from Research to Prevent Blindness to the Department of Ophthalmology, Columbia University.

Financial support

Supported in part by grants from the National Eye Institute/NIH EY024091 and a grant from Research to Prevent Blindness to the Department of Ophthalmology, Columbia University.

List of abbreviations

AF	fundus autofluorescence
AZOOR	acute zonal occult outer retinopathy

cSLO	confocal scanning laser ophthalmoscopy
GPR143/OA1	G-protein coupled receptor 143/ocular albinism-1
NIR-AF	near-infrared autofluorescence
NRPE	N-retinylidene-phosphatidylethanolamine
PE	phosphatidylethanolamine
PRPH2/RDS	peripherin-2/retinal degeneration slow
PXE	pseudoxanthoma elasticum
qAF	quantitative fundus autofluorescence
Rdh8	retinol dehydrogenase 8
RPGR	retinitis pigmentosa GTPase regulator
ROI-qAF	region-of-interest-qAF
RP	retinitis pigmentosa
RPE	retinal pigment epithelial cells
SD-OCT	spectral domain optical coherence tomography
SW	short-wavelength
SW-AF	short-wavelength fundus autofluorescence
STGD1	recessive Stargardt disease

References

Aizawa S, Mitamura Y, Hagiwara A, Sugawara T, Yamamoto S, 2010 Changes of fundus autofluorescence, photoreceptor inner and outer segment junction line, and visual function in patients with retinitis pigmentosa. Clin. Exp. Ophthalmol 38, 597–604. [PubMed: 20456441]

ANSI, 2014 American National Standard for Safe Use of Lasers. (ANSI Z136.1). Laser Institute of America, Orlando, FL.

Bakall B, Radu RA, Stanton JB, Burke JM, McKay BS, Wadelius C, Mullins RF, Stone EM, Travis GH, Marmorstein AD, 2007 Enhanced accumulation of A2E in individuals homozygous or heterozygous for mutations in BEST1 (VMD2). Exp. Eye Res 85, 34–43. [PubMed: 17477921]

Bassuk AG, Sujirakul T, Tsang SH, Mahajan VB, 2014 A novel RPGR mutation masquerading as Stargardt disease. Br. J. Ophthalmol 98, 709–711. [PubMed: 24489377]

Ben-Shabat S, Itagaki Y, Jockusch S, Sparrow JR, Turro NJ, Nakanishi K, 2002 Formation of a nona-oxirane from A2E, a lipofuscin fluorophore related to macular degeneration, and evidence of singlet oxygen involvement. Angew. Chem. Int. Ed 41, 814–817.

Bertelsen M, Zernant J, Larsen M, Duno M, Allikmets R, Rosenberg T, 2014 Generalized choriocapillaris dystrophy, a distinct phenotype in the spectrum of ABCA4-associated retinopathies. Investig. Ophthalmol. Vis. Sci 55, 2766–2776. [PubMed: 24713488]

Birnbach CD, Jarvelainen M, Possin DE, Milam AH, 1994 Histopathology and immunocytochemistry of the neurosensory retina in fundus flavimaculatus. Ophthalmology 101, 1211–1219. [PubMed: 8035984]

Bone RA, Brener B, Gibert JC, 2007 Macular pigment, photopigments, and melanin: distributions in young subjects determined by four-wavelength reflectometry. Vis. Res 47, 3259–3268. [PubMed: 17937965]

Bone RA, Landrum JT, Fernandez L, Tarsis SL, 1988 Analysis of the macular pigment by HPLC:retinal distribution and age study. Investig. Ophthalmol. Vis. Sci 29, 843–849. [PubMed: 3372161]

Boon CJ, van Schooneveld MJ, den Hollander AI, van Lith-Verhoeven JJ, Zonneveld-Vrieling MN, Theelen T, Cremers FP, Hoyng CB, Klevering BJ, 2007 Mutations in the peripherin/RDS gene are an important cause of multifocal pattern dystrophy simulating STGD1/fundus flavimaculatus. Br. J. Ophthalmol 91, 1504–1511. [PubMed: 17504850]

Borman AD, Davidson AE, O'Sullivan J, Thompson DA, Robson AG, De Baere E, Black GC, Webster AR, Holder GE, Leroy BP, Manson FD, Moore AT, 2011 Childhood-onset autosomal recessive bestrophinopathy. Arch. Ophthalmol 129, 1088–1093. [PubMed: 21825197]

Boudreault K, Schuerch K, Zhao J, Lee W, Cabral T, Yannuzzi LA, Tsang SH, Sparrow JR, 2017 Quantitative autofluorescence intensities in acute zonal occult outer retinopathy vs healthy eyes. JAMA Ophthalmol. 135, 1330–1338. [PubMed: 29075777]

Budzynski E, Gross AK, McAlear SD, Peachey NS, Shukla M, He F, Edwards M, Won J, Hicks WL, Wensel TG, Naggert JK, Nishina PM, 2010 Mutations of the opsin gene (Y102H and I307N) lead to light-induced degeneration of photoreceptors and constitutive activation of phototransduction in mice. J. Biol. Chem 285, 14521–14533.

Bunker CH, Berson EL, Bromley WC, Hayes RP, Roderick TH, 1984 Prevalence of retinitis pigmentosa in Maine. Am. J. Ophthalmol 97, 357–365. [PubMed: 6702974]

Burke TR, Duncker T, Woods RL, Greenberg JP, Zernant J, Tsang SH, Smith RT, Allikmets R, Sparrow JR, Delori FC, 2014 Quantitative fundus autofluorescence in recessive stargardt disease. Investig. Ophthalmol. Vis. Sci 55, 2841–2852. [PubMed: 24677105]

Cella W, Greenstein VC, Zernant-Rajang J, Smith TR, Barile G, Allikmets R, Tsang SH, 2009 G1961E mutant allele in the Stargardt disease gene ABCA4 causes bull's eye maculopathy. Exp. Eye Res 89, 16–24. [PubMed: 19217903]

Charbel Issa P, Barnard AR, Singh MS, Carter E, Jiang Z, Radu RA, Schraermeyer U, MacLaren RE, 2013 Fundus autofluorescence in the Abca4(−/−) mouse model of Stargardt disease–correlation with accumulation of A2E, retinal function, and histology. Investig. Ophthalmol. Vis. Sci 54, 5602–5612. [PubMed: 23761084]

Cideciyan AV, Aleman TS, Swider M, Schwartz SB, Steinberg JD, Brucker AJ, Maguire AM, Bennett J, Stone EM, Jacobson SG, 2004 Mutations in ABCA4 result in accumulation of lipofuscin before slowing of the retinoid cycle: a reappraisal of the human disease sequence. Hum. Mol. Genet 13, 525–534. [PubMed: 14709597]

Cideciyan AV, Hood DC, Huang YZ, Banin E, Li ZY, Stone EM, Milam AH, Jacobson SG, 1998 Disease sequence from mutant rhodopsin allele to rod and cone photoreceptor degeneration in man. Proc. Natl. Acad. Sci 95, 7103–7108. [PubMed: 9618546]

Cideciyan AV, Swider M, Aleman TS, Roman MI, Sumaroka A, Schwartz SB, 2007 Reduced-illuminance autofluorescence imaging in ABCA4-associated retinal degenerations. J Opt Soc Am A Opt Image Sci Vis 24, 1457–1467. [PubMed: 17429493]

Cideciyan AV, Swider M, Aleman TS, Sumaroka A, Schwartz SB, Roman MI, Milam AH, Bennett J, Stone EM, Jacobson SG, 2005 ABCA4-associated retinal degenerations spare structure and function of the human parapapillary retina. Investig. Ophthalmol. Vis. Sci 46, 4739–4746. [PubMed: 16303974]

Cideciyan AV, Swider M, Aleman TS, Tsybovsky Y, Schwartz SB, Windsor EA, Roman AJ, Sumaroka A, Steinberg JD, Jacobson SG, Stone EM, Palczewski K, 2009 ABCA4 disease progression and a proposed strategy for gene therapy. Hum. Mol. Genet 18, 931–941. [PubMed: 19074458]

Cremers FP, van de Pol DJ, van Driel M, den Hollander AI, van Haren FJ, Knoers NV, Tijmes N, Bergen AA, Rohrschneider K, Blankenagel A, Pinckers AJ, Deutman AF, Hoyng CB, 1998 Autosomal recessive retinitis pigmentosa and cone-rod dystrophy caused by splice site mutations in the Stargardt's disease gene ABCR. Hum. Mol. Genet 7, 355–362. [PubMed: 9466990]

Danciger M, Matthes MT, Yasamura D, Akhmedov NB, Rickabaugh T, Gentleman S, Redmond TM, La Vail MM, Farber DB, 2000 A QTL on distal chromosome 3 that influences the severity of light-induced damage to mouse photoreceptors. Mamm. Genome 11, 422–427. [PubMed: 10818205]

Delori F, Greenberg JP, Woods RL, Fischer J, Duncker T, Sparrow J, Smith RT, 2011a Quantitative measurements of autofluorescence with the scanning laser ophthalmoscope. Investig. Ophthalmol. Vis. Sci 52, 9379–9390. [PubMed: 22016060]

Delori FA, Duncker T, Sparrow JR, 2016a The measurement of fundus autofluorescence levels In: Lois N, Forrester JV (Eds.), Fundus Autofluorescence. Wolters Kluwer, Philadelphia, pp. 52–58.

Delori FC, 2004 Autofluorescence method to measure macular pigment optical densities fluorometry and autofluorescence imaging. Arch. Biochem. Biophys 430, 156–162. [PubMed: 15369813]

Delori FC, Dorey CK, Staurenghi G, Arend O, Goger DG, Weiter JJ, 1995a In vivo fluorescence of the ocular fundus exhibits retinal pigment epithelium lipofuscin characteristics. Investig. Ophthalmol. Vis. Sci 36, 718–729. [PubMed: 7890502]

Delori FC, Duncker T, Sparrow JR, 2016b The measurement of fundus autofluorescence levels In: Lois N, Forrester JV (Eds.), Fundus Autofluorescence. Wolters Kluwer, Philadelphia, pp. 52–58.

Delori FC, Goger DG, Dorey CK, 2001 Age-related accumulation and spatial distribution of lipofuscin in RPE of normal subjects. Investig. Ophthalmol. Vis. Sci 42, 1855–1866. [PubMed: 11431454]

Delori FC, Greenberg JP, Woods RL, Fischer J, Duncker T, Sparrow JR, Smith RT, 2011b Quantitative measurements of autofluorescence with the scanning laser ophthalmoscope. Investig. Ophthalmol. Vis. Sci 52, 9379–9390. [PubMed: 22016060]

Delori FC, Keilhauer C, Sparrow JR, Staurenghi G, 2007 Origin of fundus autofluorescence In: Holz FG, Schmitz-Valckenberg S, Spaide RF, Bird AC (Eds.), Atlas of Fundus Autofluorescence Imaging. Springer-Verlag, Berlin Heidelberg, pp. 17–29.

Delori FC, Staurenghi G, Arend O, Dorey CK, Goger DG, Weiter JJ, 1995b In vivo measurement of lipofuscin in Stargardt's disease–Fundus flavimaculatus. Investig. Ophthalmol. Vis. Sci 36, 2327–2331. [PubMed: 7558729]

Duncker T, Greenberg JP, Ramachandran R, Hood DC, Smith RT, Hirose T, Woods RL, Tsang SH, Delori FC, Sparrow JR, 2014 Quantitative fundus autofluorescence and optical coherence tomography in Best vitelliform macular dystrophy. Investig. Ophthalmol. Vis. Sci 55, 1471–1482. [PubMed: 24526438]

Duncker T, Greenberg JP, Sparrow JR, Smith RT, Quigley HA, Delori FC, 2012 Visualization of the optic fissure in short-wavelength autofluorescence images of the fundus. Investig. Ophthalmol. Vis. Sci 53, 6682–6686. [PubMed: 22956617]

Duncker T, Lee W, Jiang F, Ramachandran R, Hood DC, Tsang SH, Sparrow JR, Greenstein VC, 2018a Acute zonal occult outer retinopathy: structural and functional analysis across the transition zone between healthy and diseased retina. Retina 38, 118–127. [PubMed: 28590963]

Duncker T, Lee W, Jiang F, Ramachandran R, Hood DC, Tsang SH, Sparrow JR, Greenstein VC, 2018b ACUTE ZONAL OCCULT OUTER RETINOPATHY: Structural and Functional Analysis across the Transition Zone between Healthy and Diseased Retina. Retina.

Duncker T, Lee W, Tsang SH, Greenberg JP, Zernant J, Allikmets R, Sparrow JR, 2013a Distinct characteristics of inferonasal fundus autofluorescence patterns in stargardt disease and retinitis pigmentosa. Investig. Ophthalmol. Vis. Sci 54, 6820–6826. [PubMed: 24071957]

Duncker T, Stein GE, Lee W, Tsang SH, Zernant J, Bearelly S, Hood DC, Greenstein VC, Delori FC, Allikmets R, Sparrow JR, 2015a Quantitative fundus autofluorescence and optical coherence tomography in ABCA4 carriers. Investig. Ophthalmol. Vis. Sci 56, 7274–7285. [PubMed: 26551331]

Duncker T, Tabacaru MR, Lee W, Tsang SH, Sparrow JR, Greenstein VC, 2013b Comparison of near-infrared and short-wavelength autofluorescence in retinitis pigmentosa. Investig. Ophthalmol. Vis. Sci 54, 585–591. [PubMed: 23287793]

Duncker T, Tsang SH, Lee W, Zernant J, Allikmets R, Delori FC, Sparrow JR, 2015b Quantitative fundus autofluorescence distinguishes ABCA4-associated and non-ABCA4-associated Bull's-Eye Maculopathy. Ophthalmology 122, 345–355. [PubMed: 25283059]

Duncker T, Tsang SH, Woods RL, Lee W, Zernant J, Allikmets R, Delori FC, Sparrow JR, 2015c Quantitative fundus autofluorescence and optical coherence tomography in PRPH2/RDS- and

ABCA4-associated disease exhibiting phenotypic overlap. Investig. Ophthalmol. Vis. Sci 56, 3159–3170. [PubMed: 26024099]

Eagle RC, Lucier AC, Bernardino VB, Yanoff M, 1980 Retinal pigment epithelial abnormalities in fundus flavimaculatus. Ophthalmol. Times 87, 1189–1200.

Feeney-Burns L, Hilderbrand ES, Eldridge S, 1984 Aging human RPE: morphometric analysis of macular, equatorial, and peripheral cells. Investig. Ophthalmol. Vis. Sci 25, 195–200. [PubMed: 6698741]

Fekrat S, Wilkinson CP, Chang B, Yannuzzi L, Schatz H, Haller JA, 2000 Acute annular outer retinopathy: report of four cases. Am. J. Ophthalmol 130, 636–644. [PubMed: 11078842]

Ferrara DC, Costa RA, Tsang SH, Calucci D, Jorge R, Freund KB, 2010 Multimodal fundus imaging in Best vitelliform macular dystrophy. Graefes Arch. Clin. Exp. Ophthalmol 248, 1377–1386. [PubMed: 20414784]

Fine HF, Spaide RF, Ryan EH Jr., Matsumoto Y, Yannuzzi LA, 2009 Acute zonal occult outer retinopathy in patients with multiple evanescent white dot syndrome. Arch. Ophthalmol 127, 66–70. [PubMed: 19139340]

Fishkin N, Sparrow JR, Allikmets R, Nakanishi K, 2005 Isolation and characterization of a retinal pigment epithelial cell fluorophore: an all-trans-retinal dimer conjugate. Proc. Natl. Acad. Sci. U. S. A 102, 7091–7096. [PubMed: 15870200]

Fishman GA, Farber M, Patel BS, Derlacki DJ, 1987 Visual acuity loss in patients with Stargardt's macular dystrophy. Ophthalmology 809–814. [PubMed: 3658351]

Fleckenstein M, Schmitz-Valckenberg S, Martens C, Kosanetzky S, Brinkmann CK, Hageman GS, Holz FG, 2011 Fundus autofluorescence and spectral-domain optical coherence tomography characteristics in a rapidly progressing form of geographic atrophy. Investig. Ophthalmol. Vis. Sci 52, 3761–3766. [PubMed: 21310912]

Flynn E, Ueda K, Auran E, Sullivan JM, Sparrow JR, 2014 Fundus autofluorescence and photoreceptor cell rosettes in mouse models. Investig. Ophthalmol. Vis. Sci 55, 5643–5652. [PubMed: 25015357]

Frangieh GT, Green R, Fine SL, 1982 A histopatholgic study of Best's macular dystrophy. Arch. Ophthalmol 100, 1115–1121. [PubMed: 7092655]

Gallemore RP, Hughes BA, Miller SS, 1997 Retinal pigment epithelial transport mechanisms and their contributions to the electroretinogram. Prog. Retin. Eye Res 16, 509–566.

Gallemore RP, Steinberg RH, 1993 Light-evoked modulation of basolateral membrane Cl- conductance in chick retinal pigment epithelium: the light peak and fast oscillation. J. Neurophysiol 70, 1669–1680. [PubMed: 8283222]

Geng Y, Schery LA, Sharma R, Dubra A, Ahmad K, Libby RT, Williams DR, 2011 Optical properties of the mouse eye. Biomed. Opt. Express 2, 717–738. [PubMed: 21483598]

Gibbs D, Cideciyan AV, Jacobson SG, Williams DS, 2009 Retinal pigment epithelium defects in humans and mice with mutations in MYO7A: imaging melanosome-specific autofluorescence. Investig. Ophthalmol. Vis. Sci 50, 4386–4393. [PubMed: 19324852]

Gliem M, Muller PL, Birtel J, McGuinness MB, Finger RP, Herrmann P, Hendig D, Holz FG, Charbel Issa P, 2017 Quantitative fundus autofluorescence in pseudoxanthoma elasticum. Investig. Ophthalmol. Vis. Sci 58, 6159–6165. [PubMed: 29214314]

Gliem M, Muller PL, Finger RP, McGuinness MB, Holz FG, Charbel Issa P, 2016 Quantitative fundus autofluorescence in early and intermediate age-related macular degeneration. JAMA ophthalmology.

Gomez NM, Tamm ER, Straubeta O, 2013 Role of bestrophin-1 in store-operated calcium entry in retinal pigment epithelium. Pflüg. Arch 465, 481–495.

Greenberg JP, Duncker T, Woods RL, Smith RT, Sparrow JR, Delori FC, 2013 Quantitative fundus autofluorescence in healthy eyes. Investig. Ophthalmol. Vis. Sci 54, 5684–5693. [PubMed: 23860757]

Greenstein VC, Duncker T, Holopigian K, Carr RE, Greenberg J, Tsang SH, Hood DC, 2012 Structural and functional changes associated with normal and abnormal fundus autofluorescence in patients with retinitis pigmentosa. Retina 32, 349–357. [PubMed: 21909055]

Hartong DT, Berson EL, Dryja TP, 2006 Retinitis pigmentosa. Lancet 368, 1795–1809. [PubMed: 17113430]

Hartzell HC, Qu Z, Yu K, Xiao Q, Chien LT, 2008 Molecular physiology of bestrophins: multifunctional membrane proteins linked to best disease and other retinopathies. Physiol. Rev 88, 639–672. [PubMed: 18391176]

Holden AL, Fitzke FW, 1988 Image size in the fundus: structural evidence for widefield retinal magnification factor. Br. J. Ophthalmol 72, 228–230. [PubMed: 3355810]

Holz FG, Bellmann C, Margaritidis M, Schutt F, Otto TP, Volcker HE, 1999 Patterns of increased in vivo fundus autofluorescence in the junctional zone of geographic atrophy of the retinal pigment epithelium associated with age-related macular degeneration. Graefes Arch. Clin. Exp. Ophthalmol 237, 145–152. [PubMed: 9987631]

Hood DC, Lazow MA, Locke KG, Greenstein VC, Birch DG, 2011 The transition zone between healthy and diseased retina in patients with retinitis pigmentosa. Investig. Ophthalmol. Vis. Sci 52, 101–108. [PubMed: 20720228]

Huang Z, Zeng H, 2006 Cutaneous melanin exhibiting fluorescence emission under near-infrared light excitation. J. Biomed. Opt 11, 34010.

Hwang JC, Zernant J, Allikmets R, Barile GR, Chang S, Smith RT, 2009 Peripapillary atrophy in Stargardt disease. Retina 29, 181–186. [PubMed: 18854780]

Iwabe S, Ying GS, Aguirre GD, Beltran WA, 2016 Assessment of visual function and retinal structure following acute light exposure in the light sensitive T4R rhodopsin mutant dog. Exp. Eye Res 146, 341–353. [PubMed: 27085210]

Jampol LM, Becker KG, 2003 White spot syndromes of the retina: a hypothesis based on the common genetic hypothesis of autoimmune/inflammatory disease. Am. J. Ophthalmol 135, 376–379. [PubMed: 12614757]

Jang YP, Matsuda H, Itagaki Y, Nakanishi K, Sparrow JR, 2005 Characterization of peroxy-A2E and furan-A2E photooxidation products and detection in human and mouse retinal pigment epithelial cells lipofuscin. J. Biol. Chem 280, 39732–39739.

Jauregui R, Park KS, Duong JK, Sparrow JR, Tsang SH, 2018 Quantitative comparison of near-infrared versus short-wave autofluorescence imaging in monitoring progression of retinitis pigmentosa. Am. J. Ophthalmol 194, 120–125. [PubMed: 30053465]

Jin ML, Li S, Moghrabi WN, Sun H, Travis GH, 2005 Rpe65 is the retinoid isomerase in bovine retinal pigment epithelium. Cell 122, 449–459. [PubMed: 16096063]

Johnson AA, Guziewicz KE, Lee CJ, Kalathur RC, Pulido JS, Marmorstein LY, Marmorstein AD, 2017 Bestrophin 1 and retinal disease. Prog. Retin. Eye Res 58, 45–69. [PubMed: 28153808]

Jung JJ, Khan S, Mrejen S, Gallego-Pinazo R, Cunningham ET Jr., Freund KB, Jampol LM, Yannuzzi LA, 2014 Idiopathic multifocal choroiditis with outer retinal or chorioretinal atrophy. Retina 34, 1439–1450. [PubMed: 24378424]

Kane Dickson V, Pedi L, Long SB, 2014 Structure and insights into the function of a Ca(2+)-activated Cl(−) channel. Nature 516, 213–218. [PubMed: 25337878]

Katz ML, Redmond TM, 2001 Effect of Rpe65 knockout on accumulation of lipofuscin fluorophores in the retinal pigment epithelium. Investig. Ophthalmol. Vis. Sci 42, 3023–3030. [PubMed: 11687551]

Keilhauer CN, Delori FC, 2006 Near-infrared autofluorescence imaging of the fundus: visualization of ocular melanin. Investig. Ophthalmol. Vis. Sci 47, 3556–3564. [PubMed: 16877429]

Kellner U, Kellner S, Weber BH, Fiebig B, Weinitz S, Ruether K, 2009 Lipofuscinand melanin-related fundus autofluorescence visualize different retinal pigment epithelial alterations in patients with retinitis pigmentosa. Eye 23, 1349–1359. [PubMed: 18791550]

Kellner U, Kellner S, Weinitz S, 2010 Fundus autofluorescence (488 nm) and near-infrared autofluorescence (787 nm) visualize different retinal pigment epithelium alterations in patients with age-related macular degeneration. Retina 30, 6–15. [PubMed: 20066766]

Kim HJ, Sparrow JR, 2018 Novel bisretinoids of human retina are lyso alkyl ether glycerophosphoethanolamine-bearing A2PE species. J. Lipid Res 59, 1620–1629. [PubMed: 29986955]

Kim SR, Fishkin N, Kong J, Nakanishi K, Allikmets R, Sparrow JR, 2004 The Rpe65 Leu450Met variant is associated with reduced levels of the RPE lipofuscin fluorophores A2E and iso-A2E. Proc. Natl. Acad. Sci. U. S. A 101, 11668–11672.

Kim SR, Jang Y, Sparrow JR, 2010 Photooxidation of RPE Lipofuscin bisretinoids enhanced fluorescence intensity. Vis. Res 50, 729–736. [PubMed: 19800359]

Kim SR, Jang YP, Jockusch S, Fishkin NE, Turro NJ, Sparrow JR, 2007 The alltrans-retinal dimer series of lipofuscin pigments in retinal pigment epithelial cells in a recessive Stargardt disease model. Proc. Natl. Acad. Sci. U. S. A 104, 19273–19278.

Kim SR, Jockusch S, Itagaki Y, Turro NJ, Sparrow JR, 2008 Mechanisms involved in A2E oxidation. Exp. Eye Res 86, 975–982. [PubMed: 18439997]

Kim SR, Nakanishi K, Itagaki Y, Sparrow JR, 2006 Photooxidation of A2-PE, a photoreceptor outer segment fluorophore, and protection by lutein and zeaxanthin. Exp. Eye Res 82, 828–839. [PubMed: 16364293]

Kitiratschky VB, Grau T, Bernd A, Zrenner E, Jagle H, Renner AB, Kellner U, Rudolph G, Jacobson SG, Cideciyan AV, Schaich S, Kohl S, Wissinger B, 2008 ABCA4 gene analysis in patients with autosomal recessive cone and cone rod dystrophies. Eur. J. Hum. Genet 16, 812–819. [PubMed: 18285826]

Lee W, Schuerch K, Zernant J, Collison FT, Bearelly S, Fishman GA, Tsang SH, Sparrow JR, Allikmets R, 2017 Genotypic spectrum and phenotype correlations of ABCA4-associated disease in patients of south Asian descent. Eur. J. Hum. Genet 25, 735–743. [PubMed: 28327576]

Lengyel I, Csutak A, Florea D, Leung I, Bird AC, Jonasson F, Peto T, 2015 A population-based ultra-widefield digital image grading study for age-related macular degeneration-like lesions at the peripheral retina. Ophthalmology 122, 1340–1347. [PubMed: 25870081]

Lima de Carvalho JR Jr., Paavo M, Chen L, Chiang J, Tsang SH, Sparrow JR, 2019 Multimodal imaging in best vitelliform macular dystrophy. Investig. Ophthalmol. Vis. Sci 60, 2012–2022. [PubMed: 31070670]

Lima LH, Burke T, Greenstein VC, Chou CL, Cella W, Yannuzzi LA, Tsang SH, 2012 Progressive constriction of the hyperautofluorescent ring in retinitis pigmentosa. Am. J. Ophthalmol 153, 718–727. [PubMed: 22137208]

Lima LH, Cella W, Greenstein VC, Wang NK, Busuioc M, Smith RT, Yannuzzi LA, Tsang SH, 2009 Structural assessment of hyperautofluorescent ring in patients with retinitis pigmentosa. Retina 29, 1025–1031. [PubMed: 19584660]

Liu Z, Ueda K, Kim HJ, Sparrow JR, 2015 Photobleaching and fluorescence recovery of RPE bisretinoids. PLoS One 10, e0138081.

Lois N, Halfyard A, Bird AC, Fitzke FW, 2000 Quantitative evaluation of fundus autofluorescence imaged ‘in vivo’ in eyes with retinal disease. Br. J. Ophthalmol 84, 741–745. [PubMed: 10873986]

Lois N, Halfyard AS, Bird AC, Holder GE, Fitzke FW, 2004 Fundus autofluorescence in Stargardt macular dystrophy-fundus flavimaculatus. Am. J. Ophthalmol 138, 55–63. [PubMed: 15234282]

Lois N, Halfyard AS, Bunce C, Bird AC, Fitzke FW, 1999 Reproducibility of fundus autofluorescence measurements obtained using a confocal scanning laser ophthalmoscope. Br. J. Ophthalmol 83, 276–279. [PubMed: 10365032]

Lopez PF, Maumenee IH, de la Cruz Z, Green WR, 1990 Autosomal-dominant fundus favimaculatus. Clinicopathologic correlation. Ophthalmol 97, 798–809.

Lorenz B, Wabbels B, Wegscheider E, Hamel CP, Drexler W, Presing MN, 2004 Lack of fundus autofluorescence to 488 nanometers from childhood on in patients with early-onset severe retinal dystrophy associated with mutations in RPE65. Ophthalmol. Times 111, 1585–1594.

Lyubarsky AL, Savchenko AB, Morocco SB, Daniele LL, Redmond TM, Pugh EN, 2005 Mole quantity of RPE65 and its productivity in the generation of 11-cisretinal from retinyl esters in the living mouse eye. Biochemist 44, 9880–9888.

Maeda A, Golczak M, Maeda T, Palczewski K, 2009 Limited roles of Rdh8, Rdh12, and Abca4 in all-trans-retinal clearance in mouse retina. Investig. Ophthalmol. Vis. Sci 50, 5435–5443. [PubMed: 19553623]

Maeda A, Maeda T, Golczak M, Palczewski K, 2008 Retinopathy in mice induced by disrupted all-trans-retinal clearance. J. Biol. Chem 283, 26684–26693.

Marmor MF, McNamara JA, 1996 Pattern dystrophy of the retinal pigment epithelium and geographic atrophy of the macula. Am. J. Ophthalmol 122, 382–392. [PubMed: 8794711]

Marmorstein AD, Marmorstein LY, Rayborn M, Wang XD, Hollyfield JG, Petrukhin K, 2000 Bestrophin, the product of the Best vitelliform macular dystrophy gene (VMD2), localizes to the basolateral plasma membrane of the retinal pigment epithelium. Proc. Natl. Acad. Sci. U. S. A 97, 12758–12763.

Martinez-Mir A, Paloma E, Allikmets R, Ayuso C, del Rio T, Dean M, Vilageliu L, Gonzalez-Duarte R, Balcells S, 1998 Retinitis pigmentosa caused by a homozygous mutation in the Stargardt disease gene ABCR. Nat. Genet 18, 11–12. [PubMed: 9425888]

Maugeri A, Klevering BJ, Rohrschneider K, Blankenagel A, Brunner HG, Deutman AF, Hoyng CB, Cremers FP, 2000 Mutations in the ABCA4 (ABCR) gene are the major cause of autosomal recessive cone-rod dystrophy. Am. J. Hum. Genet 67, 960–966. [PubMed: 10958761]

McDonnell PJ, Kivlin JD, Maumenee IH, Green WR, 1986 Fundus flavimaculatus without maculopathy. A clinicopathologic study. Ophthalmology 93, 116–119. [PubMed: 3951808]

Milenkovic VM, Rohrl E, Weber BH, Strauss O, 2011 Disease-associated missense mutations in bestrophin-1 affect cellular trafficking and anion conductance. J. Cell Sci 124, 2988–2996. [PubMed: 21878505]

Moiseyev G, Chen Y, Takahashi Y, Wu BX, Ma JX, 2005 RPE65 is the isomerohydrolase in the retinoid visual cycle. Proc. Natl. Acad. Sci. U. S. A 102, 12413–12418.

Morgan JI, Pugh EN Jr., 2013 Scanning laser ophthalmoscope measurement of local fundus reflectance and autofluorescence changes arising from rhodopsin bleaching and regeneration. Investig. Ophthalmol. Vis. Sci 54, 2048–2059. [PubMed: 23412087]

Mrejen S, Khan S, Gallego-Pinazo R, Jampol LM, Yannuzzi LA, 2014 Acute zonal occult outer retinopathy: a classification based on multimodal imaging. JAMA ophthalmology 132, 1089–1098. [PubMed: 24945598]

Muller PL, Gliem M, Mangold E, Bolz HJ, Finger RP, McGuinness M, Betz C, Jiang Z, Weber BH, MacLaren RE, Holz FG, Radu RA, Charbel Issa P, 2015 Monoallelic ABCA4 mutations appear insufficient to cause retinopathy: a quantitative autofluorescence study. Investig. Ophthalmol. Vis. Sci 56, 8179–8186. [PubMed: 26720470]

Naash ML, Peachey NS, Li Z-Y, Gryczan CC, Goto Y, Blanks JC, Milam AH, Ripps H, 1996 Light-induced acceleration of photoreceptor degeneration in transgenic mice expressing mutant rhodopsin. Investig. Ophthalmol. Vis. Sci 37, 775–782. [PubMed: 8603862]

Nagiel A, Lalane RA, Sadda SR, Schwartz SD, 2016 Ultra-widefield fundus imaging: a review of clinical applications and future trends. Retina 36, 660–678. [PubMed: 27014860]

Neussert R, Muller C, Milenkovic VM, Strauss O, 2010 The presence of bestrophin-1 modulates the Ca2+ recruitment from Ca2+ stores in the ER. Pflüg. Arch 460, 163–175.

Nusinowitz S, Nguyen L, Radu RA, Kashani Z, Farber DB, Danciger M, 2003 Electroretinographic evidence for altered phototransduction gain and slowed recovery from photo-bleaches in albino mice with a MET450 variant in RPE6. Exp. Eye Res 77, 627–638. [PubMed: 14550405]

O'Gorman S, Flaherty WA, Fishman GA, Berson EL, 1988 Histopathological findings in Best's vitelliform macular dystrophy. Arch. Ophthalmol 106, 1261–1268. [PubMed: 3415551]

Paavo M, Lee W, Allikmets R, Tsang S, Sparrow JR, 2019 Photoreceptor cells as a source of fundus autofluorescence in recessive Stargardt disease. J. Neurosci. Res 97, 98–106. [PubMed: 29701254]

Paavo M, Zhao J, Kim HJ, Lee W, Zernant J, Cai C, Allikmets R, Tsang SH, Sparrow JR, 2018 Mutations in GPR143/OA1 and ABCA4 inform interpretations of short-wavelength and near-infrared fundus autofluorescence. Investig. Ophthalmol. Vis. Sci 59, 2459–2469. [PubMed: 29847651]

Papermaster DS, Schneider BG, Zorn MA, Kraehenbuhl JP, 1978 Immunocytochemical localization of a large intrinsic membrane protein to the incisures and margins of frog rod outer segment disks. J. Cell Biol 78, 415–425. [PubMed: 690173]

Parish CA, Hashimoto M, Nakanishi K, Dillon J, Sparrow JR, 1998 Isolation and one-step preparation of A2E and iso-A2E, fluorophores from human retinal pigment epithelium. Proc. Natl. Acad. Sci. U. S. A 95, 14609–14613.

Petrukhin K, Koisti MJ, Bakall B, Li W, Xie G, Marknell T, Sandgren O, Forsman K, Holmgren G, Andreasson S, Vujic M, Bergen AAB, McGarty-Dugan V, Figueroa D, Austin CP, Metzker ML, Caskey CT, Wadelius C, 1998 Identification of the gene responsible for Best macular dystrophy. Nat. Genet 19, 241–247. [PubMed: 9662395]

Popovic P, Jarc-Vidmar M, Hawlina M, 2005 Abnormal fundus autofluorescence in relation to retinal function in patients with retinitis pigmentosa. Graefe's Arch. Clin. Exp. Ophthalmol 243, 1018–1027. [PubMed: 15906064]

Qu Z, Hartzell HC, 2008 Bestrophin Cl-channels are highly permeable to HCO3-. Am. J. Physiol. Cell Physiol 294, C1371–C1377.

Querques G, Regenbogen M, Quijano C, Delphin N, Soubrane G, Souied EH, 2008 High-definition optical coherence tomography features in vitelliform macular dystrophy. Am. J. Ophthalmol 146, 501–507. [PubMed: 18619572]

Redmond TM, Poliakov E, Yu S, Tsai JY, Lu Z, Gentleman S, 2005 Mutation of key residues of RPE65 abolishes its enzymatic role as isomerohydrolase in the visual cycle. Proc. Natl. Acad. Sci. U. S. A 102, 13658–13663.

Reiter GS, Told R, Baratsits M, Hecht A, Schlanitz FG, Sacu S, Schmidt-Erfurth U, 2018 Repeatability and reliability of quantitative fundus autofluorescence imaging in patients with early and intermediate age-related macular degeneration. Acta Ophthalmol.

Renner AB, Fiebig BS, Weber BH, Wissinger B, Andreasson S, Gal A, Cropp E, Kohl S, Kellner U, 2009 Phenotypic variability and long-term follow-up of patients with known and novel PRPH2/RDS gene mutations. Am. J. Ophthalmol 147, 518–530. [PubMed: 19038374]

Robson AG, Lenassi E, Saihan Z, Luong VA, Fitzke FW, Holder GE, Webster AR, 2012 Comparison of fundus autofluorescence with photopic and scotopic fine matrix mapping in patients with retinitis pigmentosa: 4- to 8-year follow-up. Investig. Ophthalmol. Vis. Sci 53, 6187–6195. [PubMed: 22899761]

Robson AG, Michaelides M, Saihan Z, Bird AC, Webster AR, Moore AT, Fitzke FW, Holder GE, 2008 Functional characteristics of patients with retinal dystrophy that manifest abnormal parafoveal annuli of high density fundus autofluorescence: a review and update. Doc. Ophthalmol 116, 79–89. [PubMed: 17985165]

Robson AG, Saihan Z, Jenkins SA, Fitzke FW, Bird AC, Webster AR, Holder GE, 2006 Functional characterisation and serial imaging of abnormal fundus autofluorescence in patients with retinitis pigmentosa and normal visual acuity. Br. J. Ophthalmol 90, 472–479. [PubMed: 16547330]

Robson AG, Tufail A, Fitzke FW, Bird AC, Moore AT, Holder GE, Webster AR, 2011 Serial imaging and structure-function correlates of high-density rings of fundus autofluorescence in retinitis pigmentosa. Retina 31, 1670–1679. [PubMed: 21394059]

Rudnicka AR, Burk RO, Edgar DF, Fitzke FW, 1998 Magnification characteristics of fundus imaging systems. Ophthalmology 105, 2186–2192. [PubMed: 9855145]

Sanchez-Cano A, Baraibar B, Pablo LE, Honrubia FM, 2008 Magnification characteristics of the optical coherence Tomograph STRATUS OCT 3000. Ophthalmic Physiol. Opt 28, 21–28. [PubMed: 18201332]

Schuerch K, Marsiglia M, Lee W, Tsang SH, Sparrow JR, 2016 Multimodal imaging of disease-associated pigmentary changes in retinitis pigmentosa. Retina 36 (Suppl. 1), S147–S158. [PubMed: 28005673]

Schuerch K, Woods RL, Lee W, Duncker T, Delori FC, Allikmets R, Tsang SH, Sparrow JR, 2017 Quantifying fundus autofluorescence in patients with retinitis pigmentosa. Investig. Ophthalmol. Vis. Sci 58, 1843–1855. [PubMed: 28358950]

Singh R, Shen W, Kuai D, Martin JM, Guo X, Smith MA, Perez ET, Phillips MJ, Simonett JM, Wallace KA, Verhoeven AD, Capowski EE, Zhang X, Yin Y, Halbach PJ, Fishman GA, Wright LS, Pattnaik BR, Gamm DM, 2013 iPS cell modeling of Best disease: insights into the pathophysiology of an inherited macular degeneration. Hum. Mol. Genet 22, 593–607. [PubMed: 23139242]

Snodderly DM, Auran JD, Delori FC, 1984 The macular pigment. II: spatial distribution in primate retinas. Investig. Ophthalmol. Vis. Sci 25, 674–685. [PubMed: 6724837]

Solbach U, Keilhauer C, Knabben H, Wolf S, 1997 Imaging of retinal autofluorescence in patients with age-related macular degeneration. Retina 17, 385–389. [PubMed: 9355185]

Spaide RF, 2007 Autofluorescence imaging with the fundus camera In: Holz FG, Schmitz-Valckenberg S, Spaide RF, Bird AC (Eds.), Atlas of Fundus Autofluorescence Imaging. Springer-Verlag, Berlin Heidelberg, pp. 49–54.

Spaide RF, Noble K, Morgan A, Freund KB, 2006 Vitelliform macular dystrophy. Ophthalmol. Times 113, 1392–1400.

Sparrow JR, Blonska A, Flynn E, Duncker T, Greenberg JP, Secondi R, Ueda K, Delori FC, 2013 Quantitative fundus autofluorescence in mice: correlation with HPLC quantitation of RPE lipofuscin and measurement of retina outer nuclear layer thickness. Investig. Ophthalmol. Vis. Sci 54, 2812–2820. [PubMed: 23548623]

Sparrow JR, Duncker T, Woods R, Delori FC, 2016 Quantitative fundus autofluorescence in best vitelliform macular dystrophy: RPE lipofuscin is not increased in non-lesion areas of retina. Adv. Exp. Med. Biol 854, 285–290. [PubMed: 26427423]

Sparrow JR, Gregory-Roberts E, Yamamoto K, Blonska A, Ghosh SK, Ueda K, Zhou J, 2012a The bisretinoids of retinal pigment epithelium. Prog. Retin. Eye Res 31, 121–135. [PubMed: 22209824]

Sparrow JR, Gregory-Roberts E, Yamamoto K, Blonska A, Ghosh SK, Ueda K, Zhou J, 2012b The bisretinoids of retinal pigment epithelium. Prog. Retin. Eye Res 31, 121–135. [PubMed: 22209824]

Sparrow JR, Marsiglia M, Allikmets R, Tsang S, Lee W, Duncker T, Zernant J, 2015 Flecks in recessive Stargardt disease: short-wavelength autofluorescence, near-infrared autofluorescence, and optical coherence tomography. Investig. Ophthalmol. Vis. Sci 56, 5029–5039. [PubMed: 26230768]

Sparrow JR, Vollmer-Snarr HR, Zhou J, Jang YP, Jockusch S, Itagaki Y, Nakanishi K, 2003a A2E-epoxides damage DNA in retinal pigment epithelial cells. Vitamin E and other antioxidants inhibit A2E-epoxide formation. J. Biol. Chem 278, 18207–18213.

Sparrow JR, Wu Y, Kim CY, Zhou J, 2010a Phospholipid meets all-trans-retinal: the making of RPE bisretinoids. J. Lipid Res 51, 247–261. [PubMed: 19666736]

Sparrow JR, Yoon K, Wu Y, Yamamoto K, 2010b Interpretations of fundus autofluorescence from studies of the bisretinoids of retina. Investig. Ophthalmol. Vis. Sci 51, 4351–4357. [PubMed: 20805567]

Sparrow JR, Zhou J, Ben-Shabat S, Vollmer H, Itagaki Y, Nakanishi K, 2002 Involvement of oxidative mechanisms in blue light induced damage to A2E-laden RPE. Investig. Ophthalmol. Vis. Sci 43, 1222–1227. [PubMed: 11923269]

Sparrow JR, Zhou J, Cai B, 2003b DNA is a target of the photodynamic effects elicited in A2E-laden RPE by blue light illumination. Investig. Ophthalmol. Vis. Sci 44, 2245–2251. [PubMed: 12714667]

Stamer WD, Bok D, Hu J, Jaffe GJ, McKay BS, 2003 Aquaporin-1 channels in human reitnal pigment epithelium: role in transepithelial water movement. Investig. Ophthalmol. Vis. Sci 44, 2803–2808. [PubMed: 12766090]

Steinmetz RL, Garner A, Maguire JI, Bird AC, 1991 Histopathology of incipient fundus flavimaculatus. Ophthalmology 98, 953–956. [PubMed: 1866150]

Strauss RW, Munoz B, Jha A, Ho A, Cideciyan AV, Kasilian ML, Wolfson Y, Sadda S, West S, Scholl HPN, Michaelides M, 2016 Comparison of short-wavelength reduced-illuminance and conventional autofluorescence imaging in stargardt macular dystrophy. Am. J. Ophthalmol 168, 269–278. [PubMed: 27296491]

Sujirakul T, Lin MK, Duong J, Wei Y, Lopez-Pintado S, Tsang SH, 2015 Multimodal imaging of central retinal disease progression in a 2-year mean follow-up of retinitis pigmentosa. Am. J. Ophthalmol 160, 786–798. [PubMed: 26164827]

Sun H, Nathans J, 2001 Mechanistic studies of ABCR, the ABC transporter in photoreceptor outer segments responsible for autosomal recessive Stargardt disease. J. Bioenerg. Biomembr 33, 523–530. [PubMed: 11804194]

Sun H, Smallwood PM, Nathans J, 2000 Biochemical defects in ABCR protein variants associated with human retinopathies. Nat. Genet 26, 242–246. [PubMed: 11017087]

Sun H, Tsunenari T, Yau KW, Nathans J, 2002 The vitelliform macular dystrophy protein defines a new family of chloride channels. Proc. Natl. Acad. Sci. U. S. A 99, 4008–4013. [PubMed: 11904445]

Tan AC, Sherman J, Yannuzzi LA, 2017 Acute zonal occult outer retinopathy affecting the peripheral retina with centripetal progression. Retin. Cases Brief Rep 11, 134–140. [PubMed: 27243784]

Tanaka K, Lee W, Zernant J, Schuerch K, Ciccone L, Tsang SH, Sparrow JR, Allikmets R, 2018 The rapid-onset chorioretinopathy phenotype of ABCA4 disease. Ophthalmology 125, 89–99. [PubMed: 28947085]

Tsunenari T, Sun H, Williams J, Cahill H, Smallwood P, Yau KW, Nathans J, 2003 Structure-function analysis of the bestrophin family of anion channels. J. Biol. Chem 278, 41114–41125.

Ueda K, Kim HJ, Zhao J, Song Y, Dunaief JL, Sparrow JR, 2018 Iron promotes oxidative cell death caused by bisretinoids of retina. Proc. Natl. Acad. Sci. U. S. A 115, 4963–4968. [PubMed: 29686088]

Ueda K, Zhao J, Kim HJ, Sparrow JR, 2016 Photodegradation of retinal bisretinoids in mouse models and implications for macular degeneration. Proc. Natl. Acad. Sci 113, 6904–6909. [PubMed: 27274068]

van de Kraats J, van Norren D, 2007 Optical density of the aging human ocular media in the visible and the UV. J Opt Soc Am A Opt Image Sci Vis 24, 1842–1857. [PubMed: 17728807]

van Wyk M, Schneider S, Kleinlogel S, 2015 Variable phenotypic expressivity in inbred retinal degeneration mouse lines: a comparative study of C3H/HeOu and FVB/ N rd1 mice. Mol. Vis 21, 811–827. [PubMed: 26283863]

Vaughan DK, Coulibaly SF, Darrow RM, Organisciak DT, 2003 A morphometric study of light-induced damage in transgenic rat models of retinitis pigmentosa. Investig. Ophthalmol. Vis. Sci 44, 848–855. [PubMed: 12556421]

Vedantham V, Ramasamy K, 2005 Optical coherence tomography in Best's disease: an observational case report. Am. J. Ophthalmol 139, 351–353. [PubMed: 15734003]

von Ruckmann A, Fitzke FW, Bird AC, 1995 Distribution of fundus autofluorescence with a scanning laser ophthalmoscope. Br. J. Ophthalmol 79, 407–412. [PubMed: 7612549]

von Ruckmann A, Fitzke FW, Bird AC, 1997 Fundus autofluorescence in age-related macular disease imaged with a laser scanning ophthalmoscope. Investig. Ophthalmol. Vis. Sci 38, 478–486. [PubMed: 9040481]

Watzke RC, Folk JC, Lang RM, 1982 Pattern dystrophy of the retinal pigment epithelium. Ophthalmology 89, 1400–1406. [PubMed: 6984500]

Weingeist TA, Kobrin JL, Watzke RC, 1982 Histopathology of Best's macular dystrophy. Arch. Ophthalmol 100, 1108–1114. [PubMed: 7092654]

Weiter JJ, Delori FC, Wing GL, Fitch KA, 1986 Retinal pigment epithelial lipofuscin and melanin and choroidal melanin in human eyes. Investig. Ophthalmol. Vis. Sci 27, 145–151. [PubMed: 3943941]

Weng J, Mata NL, Azarian SM, Tzekov RT, Birch DG, Travis GH, 1999 Insights into the function of Rim protein in photoreceptors and etiology of Stargardt's disease from the phenotype in abcr knockout mice. Cell 98, 13–23. [PubMed: 10412977]

Wenzel A, Grimm C, Samardzija M, Reme CE, 2003 The genetic modified Rpe65Leu$_{450}$: effect on light damage susceptibility in c-Fos-deficient mice. Investig. Ophthalmol. Vis. Sci 44, 2798–2802. [PubMed: 12766089]

Wenzel A, Reme CE, Williams TP, Hafezi F, Grimm C, 2001 The Rpe65 Leu450Met variation increases retinal resistance against light-induced degeneration by slowing rhodopsin regeneration. J. Neurosci 21, 53–58. [PubMed: 11150319]

White DA, Fritz JJ, Hauswirth WW, Kaushal S, Lewin AS, 2007 Increased sensitivity to light-induced damage in a mouse model of autosomal dominant retinal disease (vol 48, pg 1942, 2007). Investig. Ophthalmol. Vis. Sci 48 3436–3436.

Wing GL, Blanchard GC, Weiter JJ, 1978 The topography and age relationship of lipofuscin concentration in the retinal pigment epithelium. Investig. Ophthalmol. Vis. Sci 17, 601–607. [PubMed: 669891]

Wu L, Ueda K, Nagasaki T, Sparrow JR, 2014 Light damage in Abca4 and Rpe65rd12 mice. Investig. Ophthalmol. Vis. Sci 55, 1910–1918. [PubMed: 24576873]

Wu Y, Fishkin NE, Pande A, Pande J, Sparrow JR, 2009 Novel lipofuscin bisretinoids prominent in human retina and in a model of recessive Stargardt disease. J. Biol. Chem 284, 20155–20166.

Wu Y, Yanase E, Feng X, Siegel MM, Sparrow JR, 2010 Structural characterization of bisretinoid A2E photocleavage products and implications for age-related macular degeneration. Proc. Natl. Acad. Sci 107, 7275–7280. [PubMed: 20368460]

Xiao Q, Hartzell HC, Yu K, 2010 Bestrophins and retinopathies. Pflüg. Arch 460, 559–569.

Yamamoto K, Yoon KD, Ueda K, Hashimoto M, Sparrow JR, 2011 A novel bisretinoid of retina is an adduct on glycerophosphoethanolamine. Investig. Ophthalmol. Vis. Sci 52, 9084–9090. [PubMed: 22039245]

Yamamoto K, Zhou J, Hunter JJ, Williams DR, Sparrow JR, 2012 Toward an understanding of bisretinoid autofluorescence bleaching and recovery. Investig. Ophthalmol. Vis. Sci 53, 3536–3544. [PubMed: 22570342]

Yang T, Liu Q, Kloss B, Bruni R, Kalathur RC, Guo Y, Kloppmann E, Rost B, Colecraft HM, Hendrickson WA, 2014 Structure and selectivity in bestrophin ion channels. Science 346, 355–359. [PubMed: 25324390]

Yoon KD, Yamamoto K, Ueda K, Zhou J, Sparrow JR, 2012 A novel source of methylglyoxal and glyoxal in retina: implications for age-related macular degeneration. PLoS One 7, e41309.

Yoon KD, Yamamoto K, Zhou J, Sparrow JR, 2011 Photo-products of retinal pigment epithelial bisretinoids react with cellular thiols. Mol. Vis 17, 1839–1849. [PubMed: 21850158]

Yung M, Klufas MA, Sarraf D, 2016 Clinical applications of fundus autofluorescence in retinal disease. Int J Retina Vitreous 2, 12. [PubMed: 27847630]

Zhang N, Tsybovsky Y, Kolesnikov AV, Rozanowska M, Swider M, Schwartz SB, Stone EM, Palczewska G, Maeda A, Kefalov VJ, Jacobson SG, Cideciyan AV, Palczewski K, 2015 Protein misfolding and the pathogenesis of ABCA4-associated retinal degenerations. Hum. Mol. Genet 24, 3220–3237. [PubMed: 25712131]

Zhang Q, Small KW, Grossniklaus HE, 2011 Clinicopathologic findings in Best vitelliform macular dystrophy. Graefes Arch. Clin. Exp. Ophthalmol 249, 745–751. [PubMed: 21136072]

Zhang Y, Stanton JB, Wu J, Yu K, Hartzell HC, Peachey NS, Marmorstein LY, Marmorstein AD, 2010 Suppression of Ca2+ signaling in a mouse model of Best disease. Hum. Mol. Genet 19, 1108–1118. [PubMed: 20053664]

Zhao J, Kim HJ, Sparrow JR, 2017 Multimodal fundus imaging of sodium iodatetreated mice informs RPE susceptibility and origins of increased fundus autofluorescence. Investig. Ophthalmol. Vis. Sci 58, 2152–2159. [PubMed: 28395299]

Zhao J, Ueda K, Riera M, Kim HJ, Sparrow JR, 2018 Bisretinoids mediate light sensitivity resulting in photoreceptor cell degeneration in mice lacking the receptor tyrosine kinase Mer. J. Biol. Chem 293, 19400–19410.

Zhou J, Cai B, Jang YP, Pachydaki S, Schmidt AM, Sparrow JR, 2005 Mechanisms for the induction of HNE- MDA- and AGE-adducts, RAGE and VEGF in retinal pigment epithelial cells. Exp. Eye Res 80, 567–580. [PubMed: 15781285]

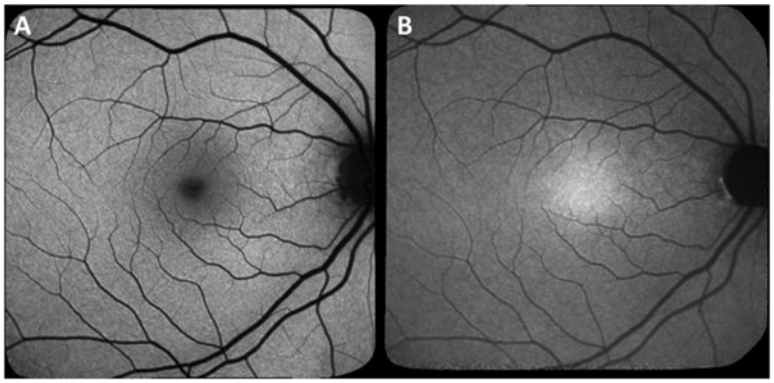

Fig. 1.

Fundus autofluorescence imaging by confocal scanning laser ophthalmoscopy. A. Short-wavelength fundus autofluorescence, 488 nm excitation. B. Near-infrared fundus autofluorescence, 787 nm excitation.

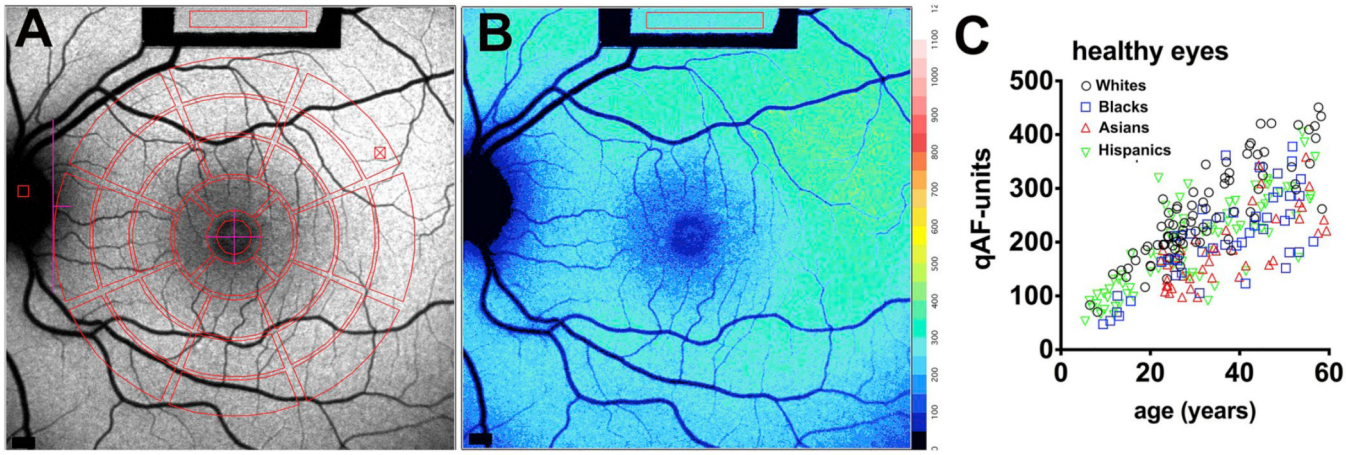

Fig. 2.

Quantitative fundus autofluorescence (qAF) in healthy eyes. A. Short-wavelength fundus autofluorescence image with overlapping measurement grid. Mean grey levels are acquired within segments (8) of three concentric rings (outer, middle, inner) and a circular foveal area. The middle ring is commonly used for quantitation as uniformity was determined to be highest in this area. Values are normalized to grey levels in the internal reference (rectangle at top of image). B. Color-coded qAF image acquired from the same eye as shown in A. Lower qAF values are coded in blue and higher levels in red (see color-code scale). C. qAF values plotted for subjects (age 5–60 years) with healthy eye status. Mean qAF_8 intensity units (qAF-units) were obtained by averaging the 8 segments in the middle ring shown in A. qAF-units are plotted as function of age; race/ethnicities of the subjects are indicated. Adapted from Greenberg et al. (2013). (For interpretation of the references to color in this figure legend, the reader is referred to the Web version of this article.)

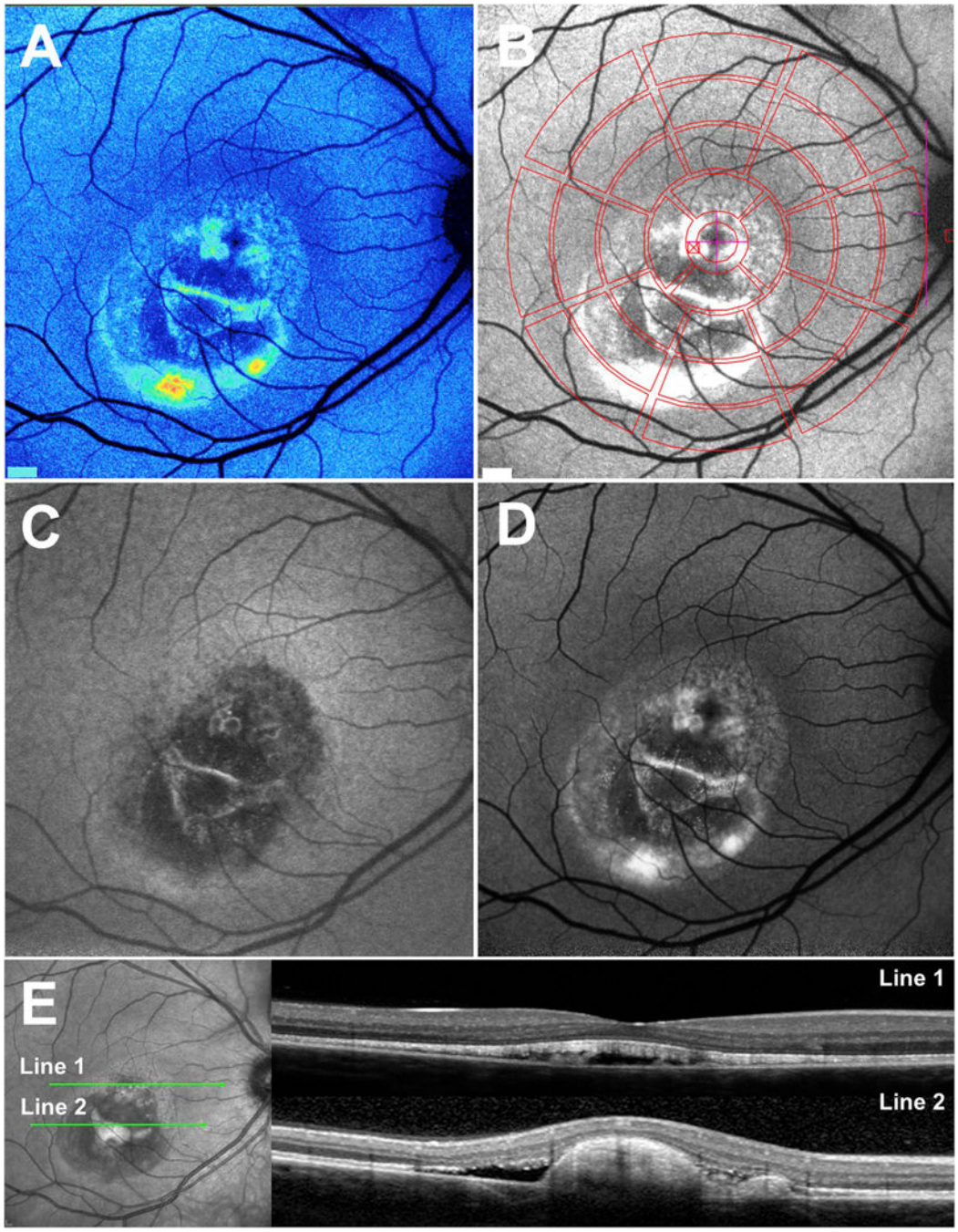

Fig. 3.

Multimodal imaging in patients exhibiting *Bestrophin-1* (*BEST1*) mutations. A. Quantitative fundus autofluorescence (qAF). Color-coded image of vitelliruptive stage. Lowest values are indicated in blue and highest values in red. B. Short-wavelength fundus autofluorescence (SW-AF) image with overlapping qAF measurement grid. Mean grey levels in the segments were normalized to the internal reference (not shown in this image). C and D. Vitelliruptive stage presented in near-infrared (NIR-AF) (C) and SW-AF (D) images. E. Spectral domain optical coherence tomography. Within the lesion (horizontal scan, line 1), the hyperreflective

interdigitation zone (IZ) is disorganized. Outer segments project into the fluid-filled lesion. Inferiorly (line 2), the hyperreflective projection is suggestive of a fibrotic scar within the central lesion. Adapted from Lima de Carvalho et al. (2019). (For interpretation of the references to color in this figure legend, the reader is referred to the Web version of this article.)

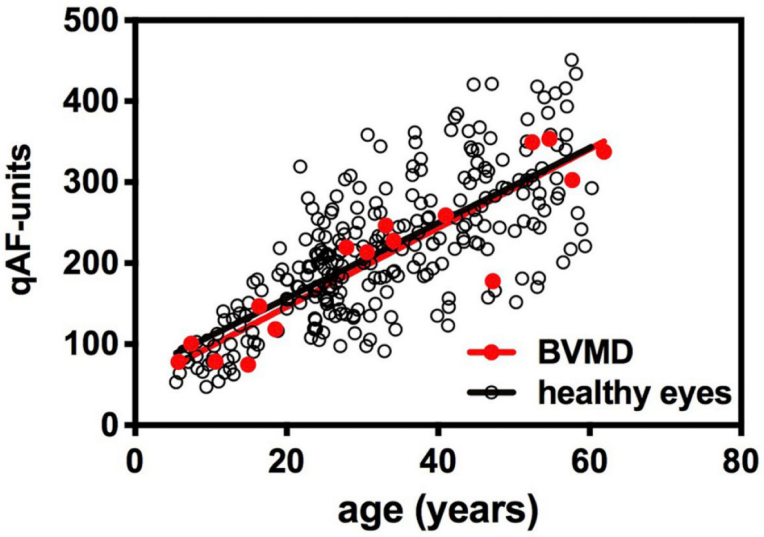

Fig. 4.

Quantitative fundus autofluorescence in Best vitelliform macular dystrophy patients (BVMD). qAF values of BVMD patients (27 eyes of 16 patients) (red circles) and healthy eyes (black open circles) are plotted as a function of age. Means are indicated by solid lines. The disease stages include: sub-clinical, 9 eyes; vitelliform, 3 eyes; pseudohypopon, 2 eyes; vitelliruptive, 12 eyes; atrophic, 1 eye. Adapted from Duncker et al. (2014). (For interpretation of the references to color in this figure legend, the reader is referred to the Web version of this article.)

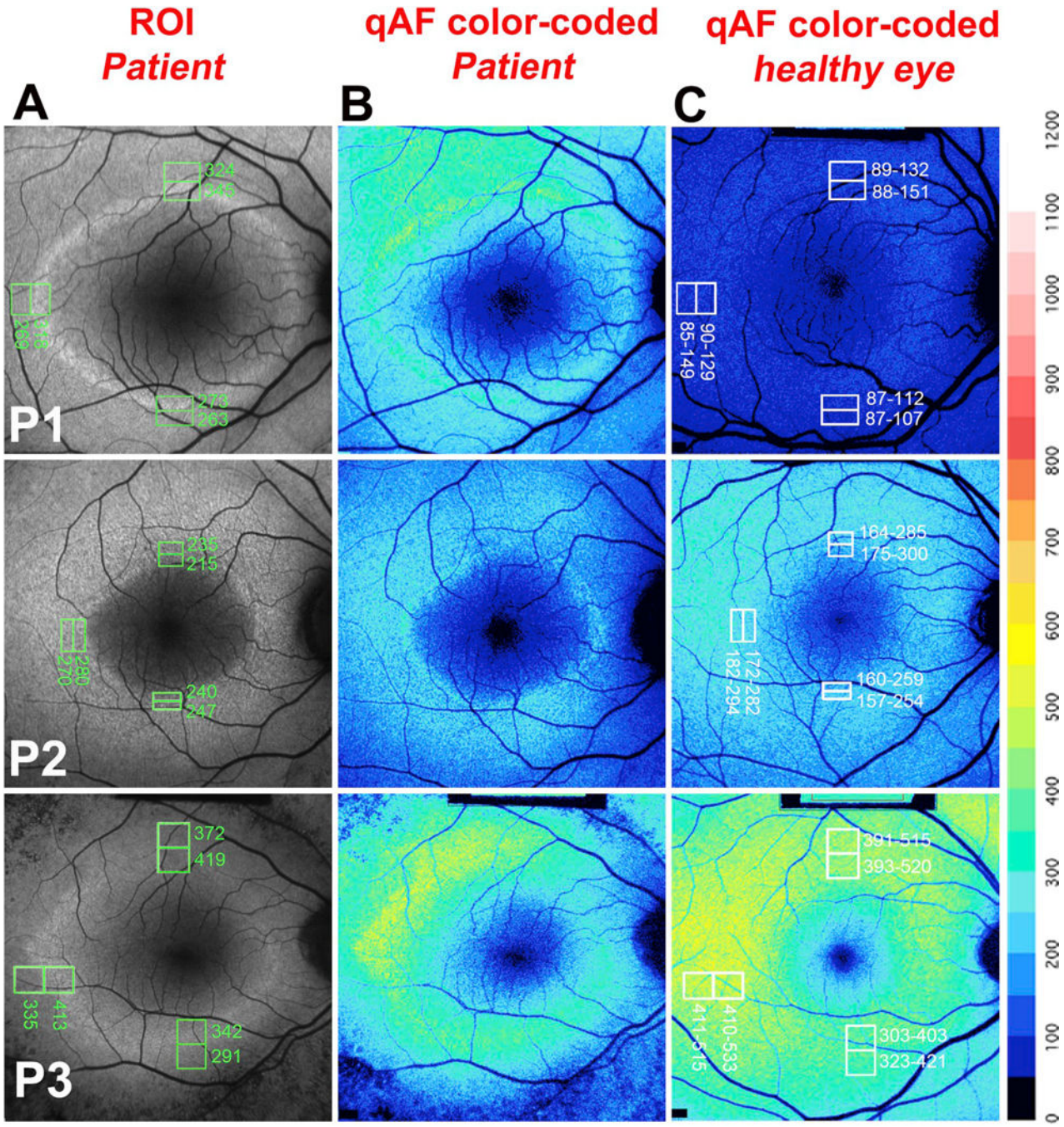

Fig. 5.

Quantitative fundus autofluorescence in retinitis pigmentosa. P, Patient. A. Representative short-wavelength fundus autofluorescence (SW-AF) images of RP patients are presented together with the positions of regions of interest (ROI) measurement areas (green rectangles) and corresponding qAF values. B. Color coded maps of qAF in patients with RP. C. Color coded maps of qAF of age-similar healthy eyes. A color scale of qAF-units (0–1200) is provided on the right margin. P1 is representative of a characteristic SW-AF ring with ROI-qAF being outside the 95% confidence (CI) of healthy individuals. P2 and P3 are examples

of patients with ROI-qAF values within the 95% CI. Adapted from Schuerch et al. (2017). (For interpretation of the references to color in this figure legend, the reader is referred to the Web version of this article.)

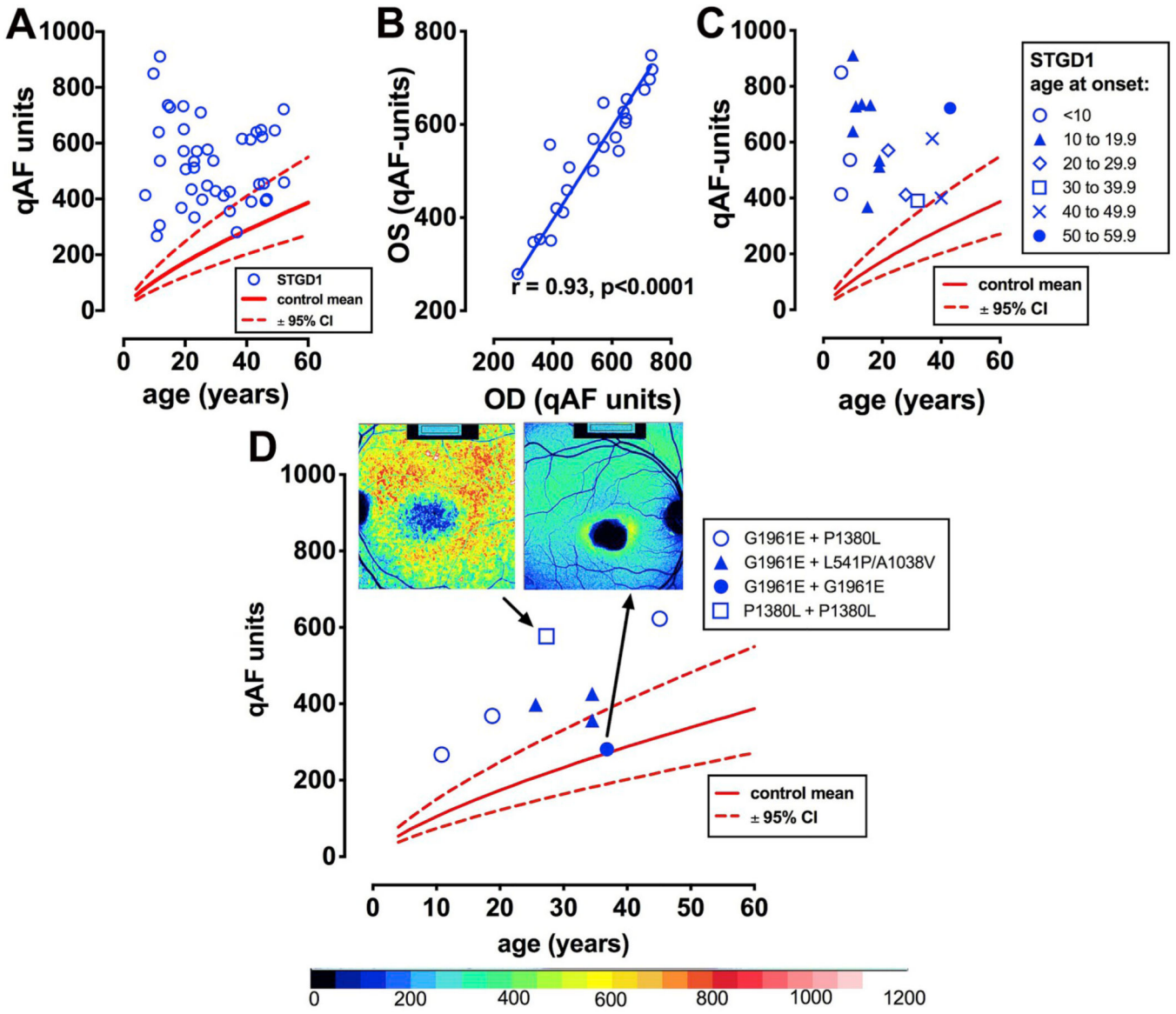

Fig. 6.

Quantitative fundus autofluorescence in recessive Stargardt disease (STGD1). A. qAF_8 values (blue circles) are plotted as a function of age. Comparison is made to mean (solid red line) and 95% confidence intervals (dashed lines) for healthy eyes. B. Linear regression analysis indicates good correspondence between left (OS) and right (OD) eyes. C. Early age of STGD1-onset can be associated with higher levels of qAF. D. qAF_8 versus age is plotted in relationship to some homozygous (p.G1961E; p. P1380L) and compound heterozygous (p.[G1961E; P1380L] [p.G1961E; p. L541/A1038V]) *ABCA4* mutations. Insets at top, color-coded images and corresponding qAF values are shown for patients carrying homozygous G1961E and P1380L mutations. Adapted from Burke et al. (2014). (For interpretation of the references to color in this figure legend, the reader is referred to the Web version of this article.)

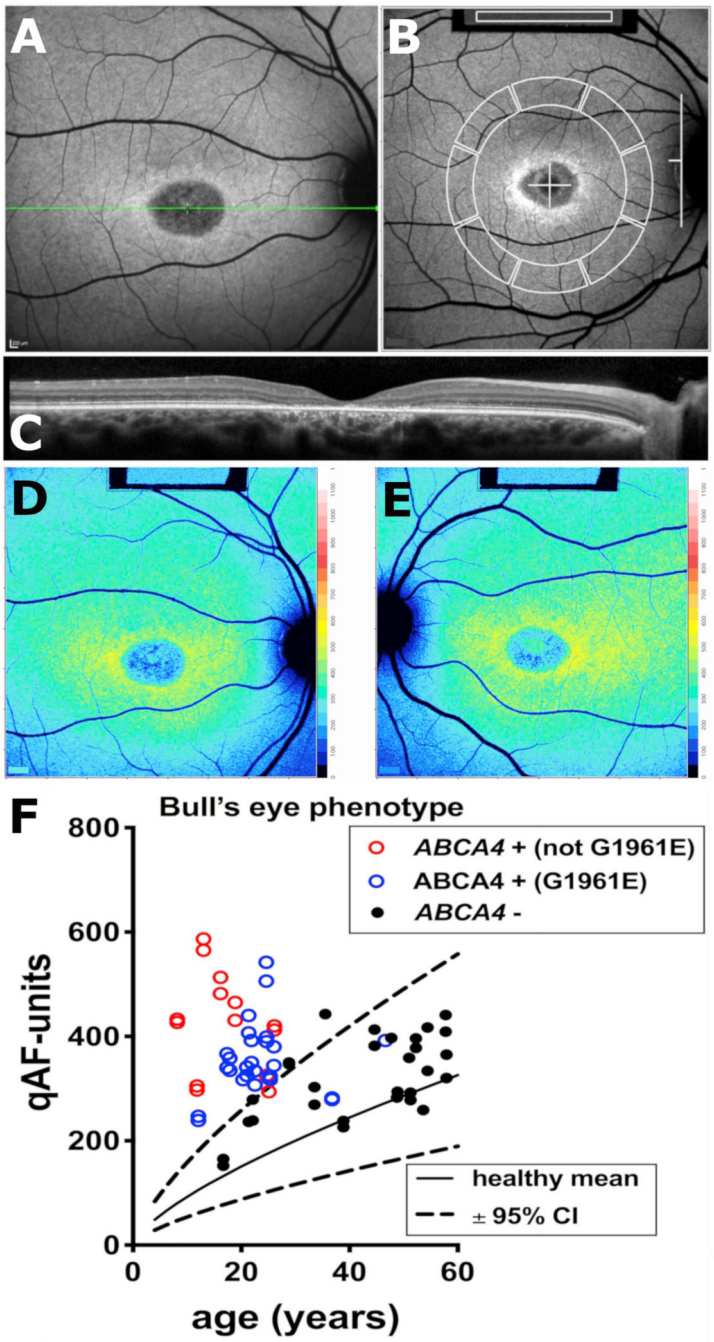

Fig. 7.

Fig. 7. Quantitative fundus autofluorescence in patients exhibiting bull's eye lesions. A. Short-wavelength fundus autofluorescence image presenting with a central bull's eye phenotype. B. qAF_8 was calculated from mean grey levels recorded within 8 circularly arranged segments positioned with 7°–9° eccentricity. Grey levels within the internal reference (rectangle, top of image) were used to correct for sensitivity and laser power. C. Spectral domain optical coherence tomography. Atrophy of the outer nuclear layer, ellipsoid zone and interdigitation zone are appreciated along with hypertransmission of signal into the

choroid. D, E. Color-coded qAF images of bull's eye lesions (OD, OS) in a patient positive for *ABCA4* mutations. Patient age 17 years. F. qAF values are plotted as a function of age for patients carrying *ABCA4* mutations (*ABCA4* +) not including the p. G1961E mutation (red circle); *ABCA4* mutations including p. G1961E (blue circles); and patients who were negative for *ABCA4* mutations (*ABCA4* -) (black symbols) but exhibited a bull's eye phenotype. Comparison is also made to mean (solid black line) and 95% confidence intervals (dashed lines) of healthy eyes. E. Adapted from Duncker et al. (2015b). (For interpretation of the references to color in this figure legend, the reader is referred to the Web version of this article.)

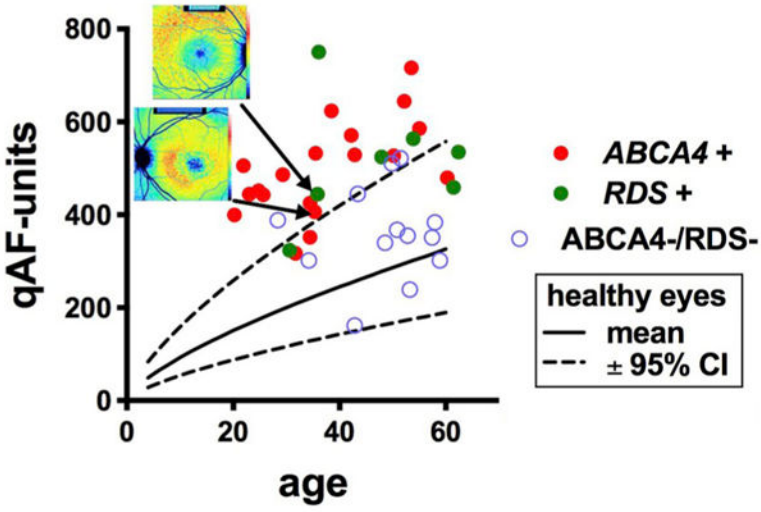

Fig. 8.

Quantitative fundus autofluorescence (qAF_8) in patients presenting with a pattern dystrophy phenotype. qAF_8 is plotted as a function of age. Genetic analysis revealed mutations in *ABCA4* (*ABCA4* +) or *peripherin2/RDS* (RDS +) or neither (*ABCA4* -/RDS-). The pattern dystrophy phenotype was defined as a central atrophy with a jagged border, mottling and flecks. Insets at top, color-coded qAF images are shown for patients carrying mutations in *ABCA4* and *RDS*. Adapted from Duncker et al. (2015c). (For interpretation of the references to color in this figure legend, the reader is referred to the Web version of this article.)

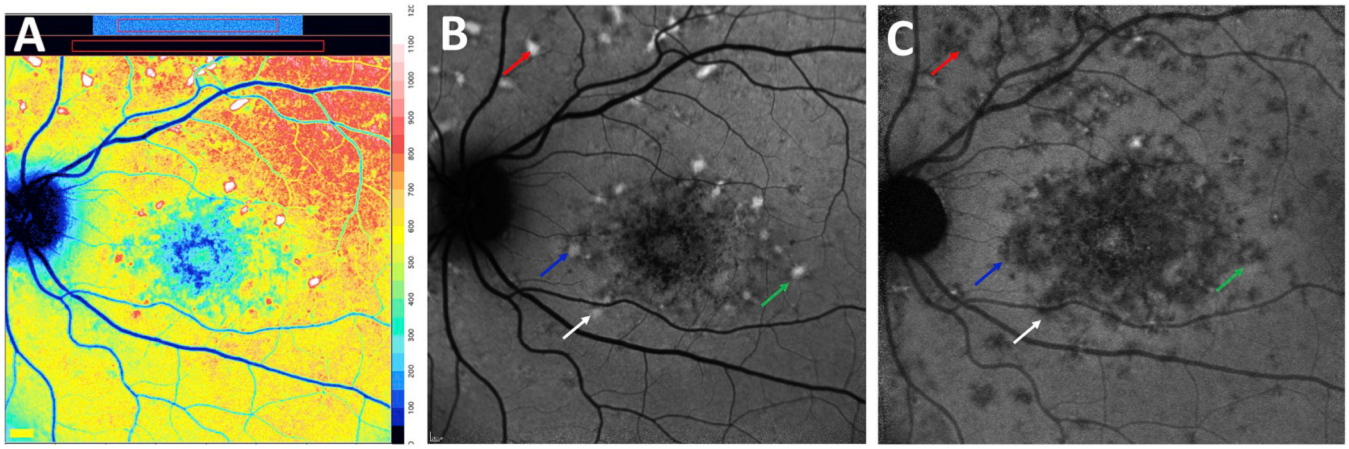

Fig. 9.

Short-wavelength (SW-AF) and near infrared fundus autofluorescence (NIR-AF) images acquired from patients with recessive Stargardt disease. A. Color-coded quantitative fundus autofluorescence image. B. SW-AF image. C. NIR-AF image. Flecks are indicated with colored arrows to denote correspondence in the SW-AF and NIR-AF modalities. Many flecks that are bright in the SW-AF image are hypoautofluorescent in the NIR-AF image. (For interpretation of the references to color in this figure legend, the reader is referred to the Web version of this article.)

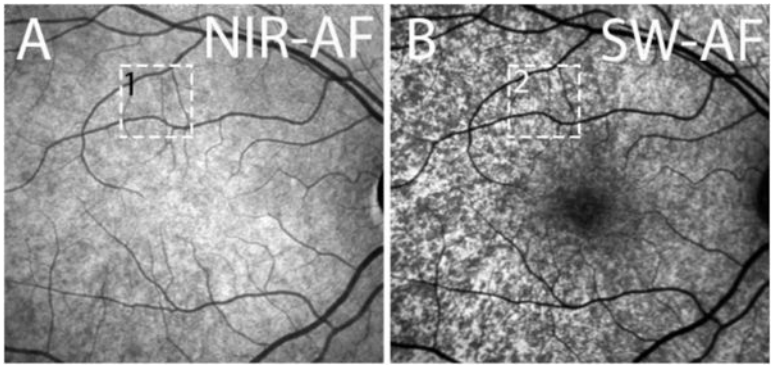

Fig. 10.

Fundus flecks in a recessive Stargardt patient. A. Flecks visualized in color-coded quantitative fundus autofluorescence images (qAF color map) (A, D) are shown together with the corresponding short-wavelength fundus autofluorescence (SW-AF, 488 nm excitation) (B, C) images. OD (A, B) and OS (C, D). Serial images were acquired at a 15-month (1, 2) and 18-month (2, 3) intervals. Note that the qAF intensity of flecks increases with time (transition from red to white coding; A1 to A2, D1 to D2) and flecks coded white have the highest qAF intensity in the images. After 18 months (A2–3; D2–3) fleck intensity faded (white transition to yellowcoded flecks). Adapted from Paavo et al. (2019). (For interpretation of the references to color in this figure legend, the reader is referred to the Web version of this article.)

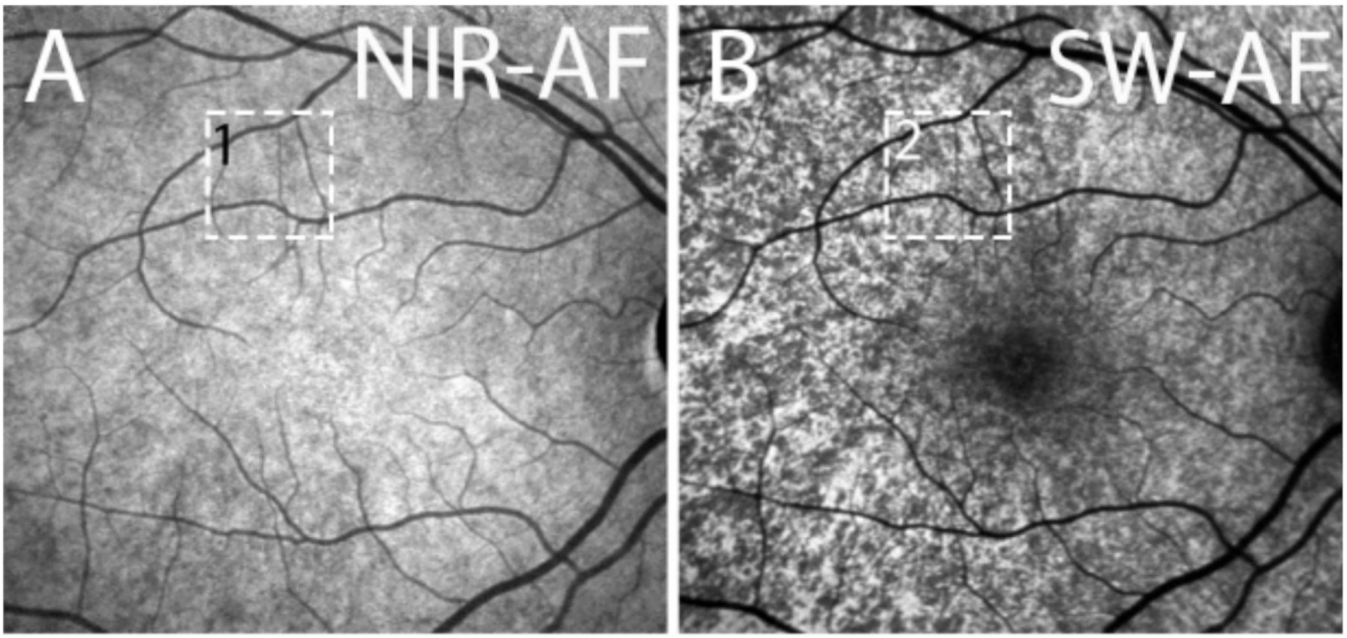

Fig. 11.

Near-infrared autofluorescence (787 nm) and short-wavelength autofluorescence (488 nm) images of a *GPR143/OA1* carrier of albinism. In NIR-AF images (A) acquired from *GPR143/OA1* carriers, the non-uniform fundus pigmentation presents centrally as patches of brightness (melanin pigment) that alternate with patches of darkness (melanin-deficient). The pattern is reversed in the SW-AF image (B). Adapted from Paavo et al. (2018).

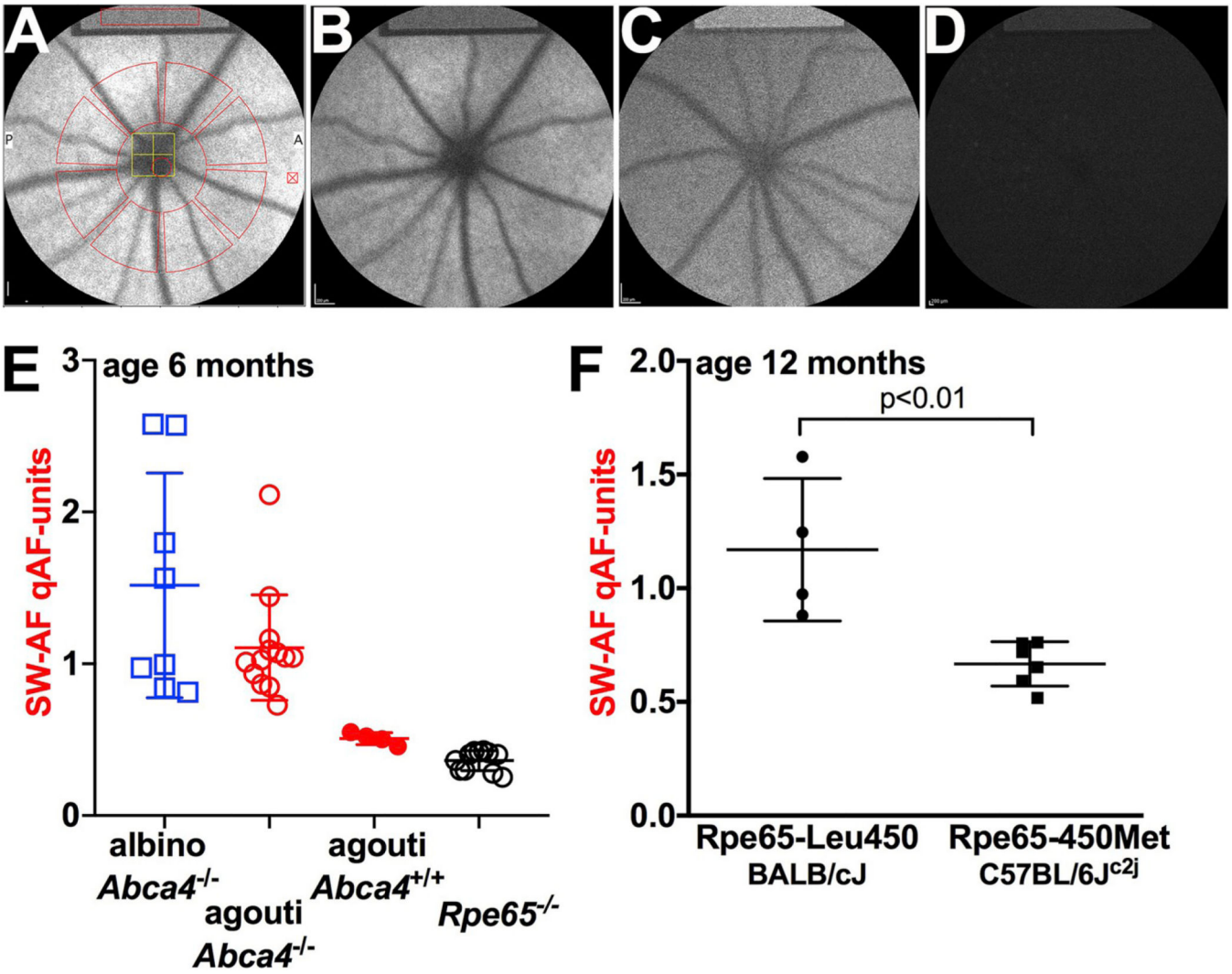

Fig. 12.

Quantitative fundus autofluorescence (qAF) in the mouse. A. Short-wavelength (SW) fundus AF image with measurement grid overlaid; the latter is used to acquire grey levels for qAF calculation. SW-AF image of agouti *Abca4*$^{-/-}$ mouse (B) agouti *Abca4*$^{+/+}$ (C) and *Rpe65*$^{-/-}$ (D). Note the internal reference (rectangle) at the top of the images. A darker reference is indicative of the use of a reduced sensitivity setting for imaging and thus higher qAF. E. qAF in mice varying in genotype (*Abca4*$^{-/-}$, *Abca4*$^{+/+}$ and *Rpe65*$^{-/-}$) and coat-color (albino, agouti, black). F. qAF is higher in *Rpe65*-Leu450 mice (BALB/cJ) than in *Rpe65*-450Met (C57BL/6Jc2j). (For interpretation of the references to color in this figure legend, the reader is referred to the Web version of this article.)

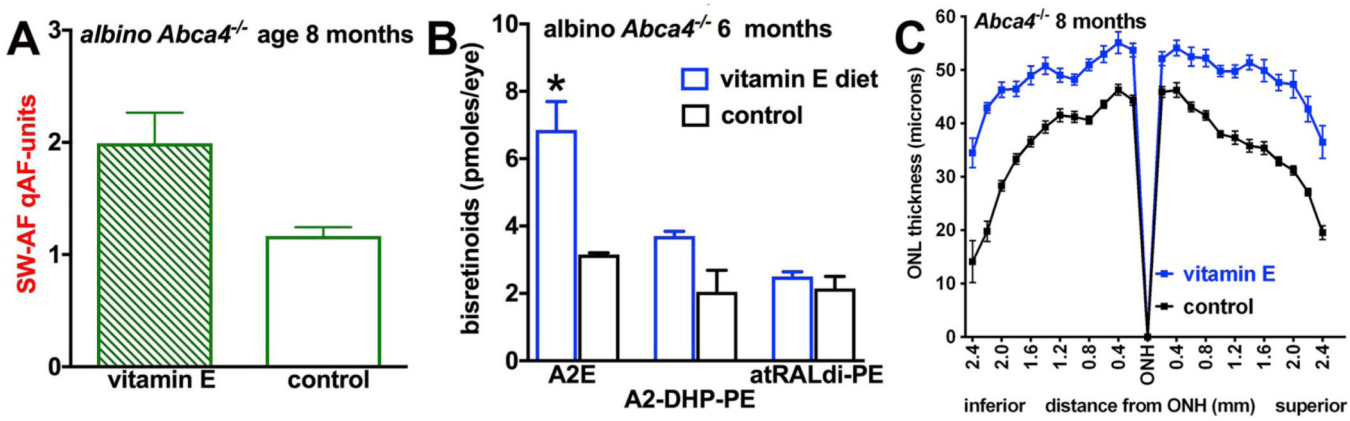

Fig. 13.

Vitamin E-mediated protection against photoxidation and photodegradation of bisretinoid in *Abca4*$^{-/-}$ mice. Vitamin E supplementation results in elevated qAF (A), elevated bisretinoid measured by HPLC (B) and reduction of the outer nuclear layer thinning characteristic of these mice (C). Adapted from Ueda et al., 2016.